NanoTherm:A Computationally Efficient EDA tool for Thermal Simulation

Thesis submitted by

Shashank Varshney
2017JVL2507

under the guidance of

Prof. Smruti Ranjan Sarangi

in partial fulfilment of the requirements
for the award of the degree of

Master of Technology

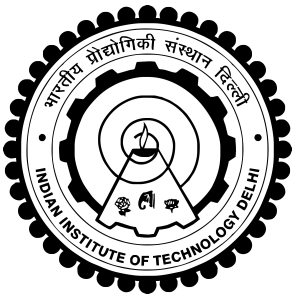

VLSI DESIGN TOOLS AND TECHNOLOGY
INDIAN INSTITUTE OF TECHNOLOGY DELHI

June 2019

THESIS CERTIFICATE

This is to certify that the thesis titled **A Computationally Efficient EDA tool for Thermal Simulation**, submitted by **Shashank Varshney**, to the Indian Institute of Technology, Delhi, for the award of the degree of **Master of Technology** in **VLSI Design Tools and Technology**, is a bona fide record of the research work done by him under my supervision. The contents of this thesis, in full or in parts, have not been submitted to any other Institute or University for the award of any degree or diploma.

Prof. Smruti Ranjan Sarangi
Dept. of Computer Science and Engineering
IIT-Delhi, 110016

Place: New Delhi

Date: 8th June 2019

ACKNOWLEDGEMENTS

I take this opportunity to thank my advisor, Dr Smruti Ranjan Sarangi, for his support and valuable guidance during the thesis. It is my fortune to have worked closely with him, who provided innumerable insight and help me stay in the course.

I would like to thank Dr Palkesh Jain (Principal Eng inner Qualcomm) for his valuable feedback on my work, and I also would like to thank Hameedah Sultan (Pursuing PhD from Dept. of Computer Science & Engineering, IIT Delhi) for all the technical discussion and suggestions.

Last but not least, I want to thank my mother Mrs Madhu Gupta for her constant encouragement and support.

ABSTRACT

KEYWORDS: Boltzmann transport equation, Nanoscale thermal simulation, Green's function, Hankel transform, Fourier equation

Temperature simulation is a classic problem in EDA, and researchers have been working on it for at least the last 15 years. In this paper, we focus on fast Green's function based approaches, where computing the temperature profile is as simple as computing the convolution of the power profile with the Green's function. We observe that for many problems of interest the process of computing the Green's function is the most time consuming phase, because we need to compute it with the slower finite difference or finite element based approaches. In this paper we propose a solution, *NanoTherm*, to compute the Green's function for an SoC very quickly using a fast analytical approach that exploits the symmetry in the thermal distribution.

Secondly, conventional analyses based on the Fourier's heat transfer equation fail to hold at the nanometer level. To accurately compute the temperature at the level of a standard cell, it is necessary to solve the Boltzmann transport equation (BTE) that accounts for quantum mechanical effects. This research area is very sparse. Conventional approaches ignore the quantum effects, which can result in a 25 to 60% error in temperature calculation. Hence, we propose a **fast analytical approach** to solve the BTE and obtain an exact solution in the Fourier transform space.

Using our fast analytical models, we demonstrate a speedup of 7-668X over state of the art techniques with an error limited to 3% while computing the combined Green's function (that incorporates both Fourier and BTE models).

Contents

List of Tables

List of Figures

Chapter 1

Introduction

For at least the last 15 years, the design community has viewed on-chip temperature as one of the most important criteria while designing a new SoC. High temperatures result in several adverse effects. The reliability of the device is negatively affected [4] and the carrier mobility is degraded, resulting in poorer performance [4]. Moreover, the chip temperature determines the leakage power. Finally, note that with increasing power and transistor densities, the problem of high on-chip temperatures is expected to get worse [5].

Different stages of the design process have different levels of information available, and the requirements for thermal optimization at each stage are different. For instance, at the architecture level, standard cell information or package level information such as the properties of the heat spreader and heat sink may not be available. Hence designers make assumptions about the missing information, and evaluate the design space from a thermal point of view. After synthesis and standard cell mapping, designers can conduct more accurate thermal analyses to determine the nature of packaging and expected on-chip temperatures for different workloads. The latter can be conveyed to software and systems designers such that they can optimize the system at their end. Over the entire design cycle, thousands of candidate designs have to be evaluated based on the information available at each stage to determine the optimal configuration. In such a case the speed of the thermal simulation becomes a bottleneck in the design process [6, 7]. As a result, **fast thermal estimation** at all stages of the design is necessary.

Many thermal simulators [8, 9, 10, 11] which are based on the classical Fourier heat transfer equation exist in this space. They can broadly be divided into three categories in decreasing order of their computation time: finite element based (FEM), finite difference

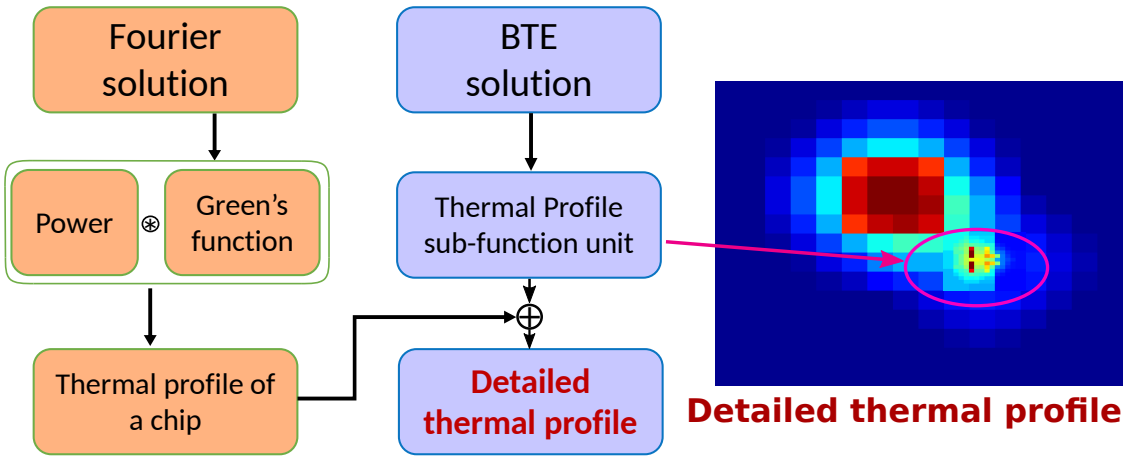

Figure 1.1: Overview of our algorithm

based (FDM), and Green's function based. The Green's function is defined as the impulse response of a unit power source (Dirac delta function). Green's function based temperature estimators [9, 10, 1] are the fastest and their accuracy is broadly acceptable [10]. We shall focus on such simulators in this paper. The main drawback of many of the Green's function based approaches is that they rely on a traditional finite element or finite difference based simulator to compute the Green's functions [9, 10, 12]. If the geometry of the chip or the boundary conditions change, the Green's function will have to be recomputed, making it a very slow and time consuming process [7]. Moreover, as we move down to smaller dimensions, at the nanometer scale, the quantum effects become significant. Conventional approaches do not take the quantum effects into account, and do a regular analysis based on classical Fourier's heat transfer equations. It has been shown in [13, 14, 15] and in our analysis that this leads to a 25 to 60% error in estimation.

Particularly, in the later stages of the design process, an accurate estimate of temperature is needed at the nanometer scale for two reasons: 1) to optimize the design of standard cells by taking thermal effects into account, and 2) to design mixed-signal blocks, where the analog functional units are highly sensitive to temperature [2].

We address both of these drawbacks of existing works by proposing a new simulator, *NanoTherm*. Figure 1.1 provides an overview of our algorithm.

1. First, we propose a very fast analytical method to compute the transient and steady state Green's functions for a conventional chip using traditional heat transfer mechanisms. Unlike prior work [1, 2] we use the notion of symmetry to reduce an $O(N^2)$ problem to an $O(N)$ problem, and then use a Hankel transform based approach.

Sadly, this is not enough to model modern SoCs, where the feature size is approaching the ballistic limit (mean free path of phonons, approximately 40 nm [15]) and quantum effects such as phonon propagation and scattering dominate at the nanoscale level. These phonon effects need to be modeled in addition to the Fourier heat equation, by solving the Boltzmann transport equation (BTE). Other than a few proposals such as ThermalScope [16, 13], there is very little work in this area.

2. The second part of our model proposes a new way of computing the temperature profile at the nanometer level using the BTE. Instead of using the finite element method as used by ThermalScope [16, 13], we derive the Green's function incorporating phonon effects by using a fast analytical approach, and finally combine the results of both Fourier and BTE based analysis. Using this approach we can derive the Green's function and the resultant temperature profile for the entire system. To the best of our knowledge, this is the first fully analytical approach to generate such a combined Green's function. Our approach, *NanoTherm*, is 7-688 times faster than the state of the art.

In Chapter 2 we introduce the relevant background and related work. Then we discuss our methodology in Chapter 3. We proceed to Chapter 4 to present the evaluation of our proposed approach and the results obtained, and finally conclude in Chapter 5.

Chapter 2

Background and Related Work

2.1 Background of Heat Transfer

The classical Fourier equation is used to solve heat transfer problems in solids. It does not model quantum effects and is meant to be used in scenarios where the geometry is orders of magnitude larger than the mean free path of phonons. It is given by:

$$\rho c \frac{\partial T}{\partial t} - k\nabla^2 T = q_{vol}, \tag{2.1}$$

where, k is the thermal conductivity, ρ is the density, c is the specific heat, and q_{vol} is the volumetric heat. The temperature field is represented by T, and time is represented by t.

This equation is typically solved using either finite element (FEM) or finite difference methods (FDM). In the FEM technique, we divide a 3D region into small blocks, and solve the heat transfer equation for each small block by either finding an analytical solution, or by choosing a function from a set of many trial functions that minimize the residual error. These equations are then combined into a global system of equations, which are solved using regular matrix methods. In the case of the finite difference method, we replace the differential equations with a set of algebraic equations. They are similar to recurrence relations, and are solved using linear algebra techniques. For example, we replace $df(x)/dt$ with $(f(x+h) - f(x))/\Delta t$, where Δt and h tend to 0. A very important offshoot of finite difference methods comprise techniques that model a temperature estimation problem as an analogous electrical circuit simulation problem (HotSpot [8] and 3D-ICE [11]).

2.1.1 Green's Function based Techniques

Both the finite difference and finite element methods require matrix inversion, which has a time complexity of $O(N^{2.37})$, making it a slow process.A faster way of computing the thermal profile is the Green's function based technique [9, 10, 1, 2]. A Green's function is defined as the impulse response of a unit power function. This can be obtained by applying 1 W of power to a very small area (approximating the Dirac delta function). The resultant temperature distribution is the Green's function, G. The advantage of this approach is that we can pre-compute and store the Green's functions, and then quickly use them at runtime

to compute the temperature profile for a given power profile. This can be done as follows:

$$T = P \circledast G, \tag{2.2}$$

where, P is the power field, and $\circledast$ is the convolution operator. There are many proposals [10, 9] that use Green's functions to speed up power estimation. However, these techniques still rely on traditional FEM and FDM based techniques to compute the Green's function in the first place. This is a very slow process. In situations where thousands of geometries have to be evaluated, the time taken in computing the Green's function will dominate the total modeling time. Hence, the main aim in this paper *is to very quickly compute the Green's function for a given geometry.*

2.1.2 Geometry of the Chip

Let us now look at the geometry of a typical chip (shown in Figure 3.1a).

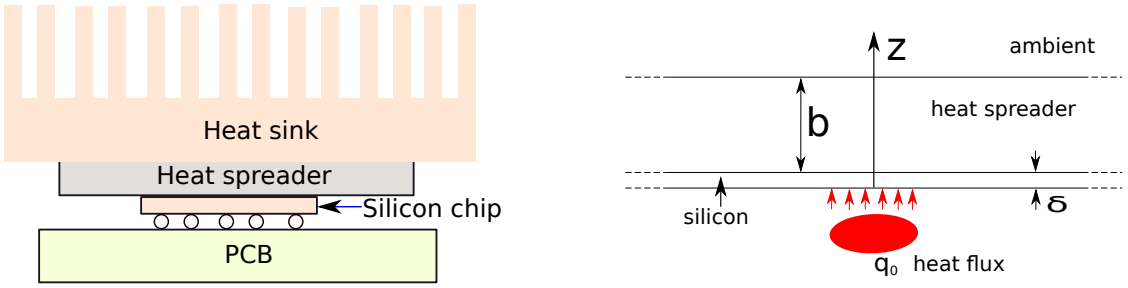

(a) (b)

Figure 2.1: (a) Layout of a package (b) Approximated model [1]

We have a layer of silicon that contains all the transistors. Over that, we have a heat spreader, which is made of a high thermal conductivity material. This helps spread the heat and reduce the formation of thermal hot spots. Above the heat spreader, we have a heat sink that has multiple fins to increase the surface area. We can use an approximate model where we remove the heat sink and substitute an iso-thermal layer in its place; this is a standard approximation made by other authors as well [1, 2]. In any case, extending our model to include the heat sink is trivial.

2.2 Boltzmann Transport Equation (BTE)

Atoms in a silicon substrate are arranged as a lattice. Synchronized perturbation of groups of atoms from their equilibrium positions is known as a vibration. The propagation of this vibration is known as a lattice wave (also known as *phonons*). This vibrational wave has

a wavelength and a velocity. From wave-particle duality, phonons also behave as particles in the quantum mechanical sense. At the nanometer scale, phonons play an important role in determining the temperature distribution. Phonons are created because of thermal fluctuations, and can be absorbed, or can get dispersed while propagating through the silicon lattice. Hence, modeling phonon creation and dispersion is crucial to estimate the temperature at the nanometer scale. The distance that phonons travel before losing their energy is of the order of several mean free paths (∼40–300 nm) [15]. When the dimensions under consideration are smaller than the mean free path, the phonon effects become significant. Hence, in modern day devices, where the device feature size is lower than the mean free path of phonons, modeling these effects is necessary to estimate temperature accurately.

To model the nanometer scale phonon effects, we typically use the molecular dynamics method, ballistic-diffusive method, or the Boltzmann transport equation. We shall focus on the Boltzmann transport equation (BTE) because it is relatively less computationally intensive and more accurate than other methods [17]. They model the heat transfer by modeling the scattering of phonons [18, 14, 19]. Specifically, we consider the gray BTE model that assumes a single mean frequency of phonons (refer to [20]):

$$\frac{\partial e_w}{\partial t} + \vec{\mathbf{v}}_g.\nabla e_w - \frac{Q}{4\pi} = \Big(\frac{\partial e_w}{\partial t}\Big)_{collision}, \tag{2.3}$$

where, e_w is the energy density function per unit solid angle, $\vec{\mathbf{v}}_g$ is the group velocity of phonons, t is the time, and Q is the volumetric heat generation. The term on the RHS models the scattering of phonons [20, 18].

2.3 Related Work

2.3.1 Green's Functions

The most influential work in analytically computing the Green's function has been done by Zhan et al. [1, 2]. They compute the Green's function by dividing a chip into multiple layers and solving the Fourier equation. They assume that the Green's function consists of a sum of cosine based basis functions. Then they find the parameters of these basis functions for different settings. This takes $O(N^2 log(N))$ time primarily because the representation of the Green's function is generic, and the isotropic nature of heat spreading is not exploited. Also, they have not modeled the transient temperature profile. *NanoTherm* instead uses the Hankel transform to solve the Fourier equation. This reduces the complexity under consideration to $O(N)$ by leveraging the symmetry of the heat distribution. Our technique is also capable of modeling the transient temperature distribution. Other analytical Green's function based techniques [21] are not capable of computing the transient temperature profile.

2.3.2 Fourier Analysis

In HotSpot [8], the authors divide the volume into small blocks and create an equivalent electrical circuit, and then solve it using matrix solvers. Coşkun et al. [22] use a similar method to solve the Fourier equation and model liquid cooling. 3DICE [11] implements a similar approach; and also models microchannels. All of these popular tools solve the Fourier equation only.

2.3.3 Solutions of the BTE

Hua et al. [14] solve a different variant of the BTE equation analytically, where they assume that the relaxation time and the specific heat are dependent on the frequency of phonons. We did not use this approach because this increases the simulation time significantly, and does not have commensurate gains in accuracy. Zahiri et al. [20] solve the gray BTE model by transforming the BTE equation into a set of ordinary differential equations. Our approach gives an exact solution in the Fourier transform space, and thus is more efficient than solving a system of differential equations. ThermalScope [16, 13] is the most related work because it takes into account both the Fourier and BTE models. It solves the gray BTE model (similar to *NanoTherm*) at the nanometer scale, and solves the Fourier equation at the level of the chip. They solve the gray BTE model using FEM and the discrete ordinate method (DOM). The slowest part of the algorithm is the FEM-based analysis, and this makes it orders of magnitude slower than our approach.

Chapter 3

Methodology

3.1 Fourier Analysis

Consider the basic system layout of an air-cooled processor, as shown in Figure 1a. We have a silicon layer that contains all the transistors. Over that we have a thermal insulating material (TIM) which fills the air gap between the silicon die and the heat spreader and helps in better heat conduction. Above that, a heat spreader (made of high conductivity Copper-Nickel alloy) is present which distributes the heat uniformly and alleviates the formation of hotspots. Over the heat spreader, we have a heat ex-changer, also known as a heat sink, which has multiple fins to increase the surface area. We can use an approximated model for simplification, where we replace the heat sink with an isothermal layer (maintained at the ambient temperature (T_a)) placed at the top of heat spreader (see Figure 3.1b); this is a standard approximation used by other authors as well [1, 2, 12].

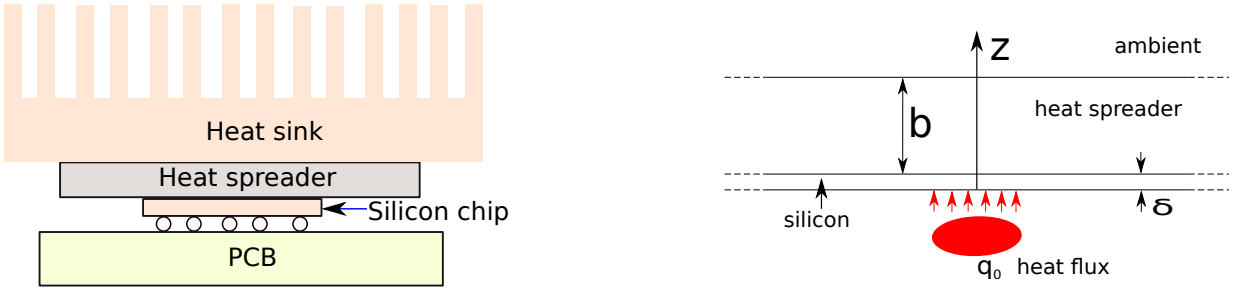

(a) (b)

Figure 3.1: (a) Layout of a package (b) Approximated model [1, 2, 3]

Table 3.1 lists all the abbreviations used.

All the architectural simulators solve the classical Fourier heat equation given by:

$$\rho_l c_l \frac{\partial T_l}{\partial t} + \nabla.(-k_l \nabla T_l) = q_{vol}, \tag{3.1}$$

where T_l is the temperature field, k_l is the thermal conductivity, ρ_l is the density, c_l is the heat capacity, ∇^2 is the Laplacian operator, q_{vol} is the volumetric heat generation, and the subscript l represents the layer number of the model. In our model we have two layers: 1) silicon die ($l = 1$) 2) heat spreader ($l = 2$). Let us expand Equation 3.1 using cylindrical co-ordinates. We will get:

Table 3.1: Glossary

Symbol	Full Form	Meaning
b		Thickness of the heat spreader
δ		Thickness of the silicon die
k		Thermal Conductivity
σ		Hankel domain
s		Laplace domain
$\boldsymbol{x}$	Boldface	Laplace Transform
$\bar{}$	Overline	Hankel Transform
$\sim$	Tilde	Fourier Transform

$$-\rho_l c_l\left(\frac{\partial T_l}{\partial t}\right)+\frac{1}{r}\frac{\partial}{\partial r}\left(r.k_l\frac{\partial T_l}{\partial r}\right)+\frac{\partial}{\partial \theta}\left(k_l\frac{\partial T_l}{\partial \theta}\right)+\frac{\partial}{\partial z}\left(k_l\frac{\partial T_l}{\partial z}\right)+q_{vol}=0. \tag{3.2}$$

The popular architectural thermal simulators like HotSpot [8], 3D-ICE [11], LightSim [10] and others [13, 16, 9, 23] model the transistors as heat sources placed at the bottom of the silicon die. The term volumetric heat generation (q_{vol}) in Equation 3.2 will be zero since the heat generation inside the silicon die is zero.

$$-\rho_l c_l\left(\frac{\partial T_l}{\partial t}\right)+\frac{1}{r}\frac{\partial}{\partial r}\left(r.k_l\frac{\partial T_l}{\partial r}\right)+\frac{\partial}{\partial \theta}\left(k_l\frac{\partial T_l}{\partial \theta}\right)+\frac{\partial}{\partial z}\left(k_l\frac{\partial T_l}{\partial z}\right)=0. \tag{3.3}$$

The thermal conductivity of the silicon die and the heat spreader is uniform in all directions. For any l^{th} layer of the model (see Figure 3.1b) Equation 3.3 will transform into Equation 3.4.

$$-\frac{\rho_l c_l}{k_l}\left(\frac{\partial T_l}{\partial t}\right)+\frac{1}{r}\frac{\partial}{\partial r}\left(r\frac{\partial T_l}{\partial r}\right)+\frac{\partial}{\partial \theta}\left(\frac{\partial T_l}{\partial \theta}\right)+\frac{\partial}{\partial z}\left(\frac{\partial T_l}{\partial z}\right)=0. \tag{3.4}$$

Since we are solving for a small circular source placed at the center of the chip, the resulting temperature distribution function will be radially symmetric (see Figure 3.2). Hence the third term on the RHS will be zero. Equation 3.4 will reduce to Equation 3.5.

$$-\frac{\rho_l c_l}{k_l}\left(\frac{\partial T_l}{\partial t}\right)+\frac{1}{r}\frac{\partial}{\partial r}\left(r\frac{\partial T_l}{\partial r}\right)+\frac{\partial}{\partial z}\left(\frac{\partial T_l}{\partial z}\right)=0. \tag{3.5}$$

Applying the product rule to the second term, Equation 3.5 will become:

$$-\frac{\rho_l c_l}{k_l}\left(\frac{\partial T_l}{\partial t}\right)+\frac{\partial^2 T_l}{\partial r^2}+\frac{1}{r}\frac{\partial T_l}{\partial r}+\frac{\partial^2 T_l}{\partial z^2}=0. \tag{3.6}$$

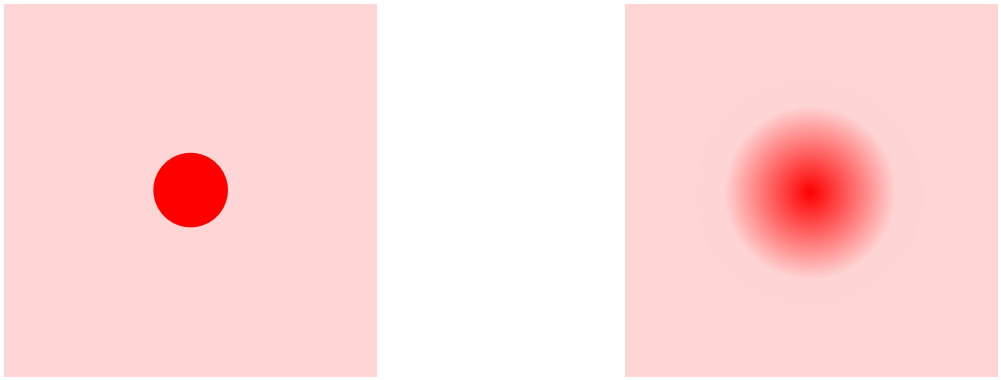

(a) (b)

Figure 3.2: (a) Circular source (b) Temperature distribution

$$-\frac{\rho_l c_l}{k_l}\left(\frac{\partial T_l}{\partial t}\right)+\underbrace{\left(\frac{\partial^2}{\partial r^2}+\frac{1}{r}\frac{\partial}{\partial r}\right)}_{\substack{\text{Zero order Bessel}\\ \text{differential operator}}}T_l+\frac{\partial^2 T_l}{\partial z^2}=0. \tag{3.7}$$

The second term on the left hand side of Equation 3.7 is the zero order Bessel differential operator and it is given in Equation 3.8 [24].

$$\nabla_o \equiv \frac{\partial^2}{\partial r^2}+\frac{1}{r}\frac{\partial}{\partial r}. \tag{3.8}$$

Thus, Equation 3.7 will become:

$$\boxed{-\frac{\rho_l c_l}{k_l}\left(\frac{\partial T_l}{\partial t}\right)+\nabla_o T_l+\frac{\partial^2 T_l}{\partial z^2}=0.} \tag{3.9}$$

3.1.1 Boundary conditions:

For the system layout shown in Figure 3.1b the boundary conditions are as follows:

1. For a circular source of radius r_o, the heat flux for $|r| \leq r_o$ is q_o, and for $|r| > r_o$ the heat flux is zero.
$$-k_1\frac{\partial T_1}{\partial z}\Big|_{z=0}=\begin{cases}q_o, & \text{for } |r|\leq r_o,\\ 0, & \text{otherwise.}\end{cases} \tag{3.10}$$
2. Heat flux at the interface of the silicon die and the heat spreader is equal.
$$-k_1\frac{\partial T_1}{\partial z}\Big|_{z=\delta}=-k_2\frac{\partial T_2}{\partial z}\Big|_{z=\delta}. \tag{3.11}$$

3. The temperature at the interface of the silicon die and the heat spreader is equal.

$$T_1(r,z)\Big|_{z=\delta} = T_2(r,z)\Big|_{z=\delta}. \tag{3.12}$$

4. The temperature at the top of the heat spreader is uniformly distributed, and it is maintained at the ambient temperature, T_a.

$$T_2(r,z)\Big|_{z=\delta+b} = T_a. \tag{3.13}$$

5. Thermal symmetry is present at r = 0, as shown in Figure 3.3. Thus we can write:

$$-k_1 \frac{\partial T_l}{\partial r}\Big|_{r=0} = 0. \tag{3.14}$$

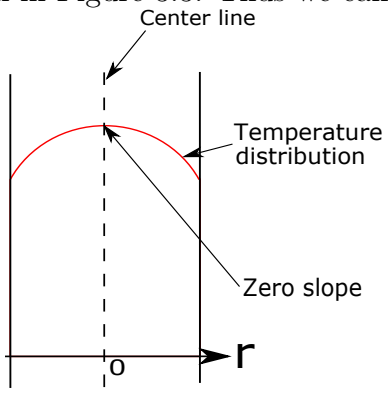

Figure 3.3: Thermal symmetry

6. For very large r, the temperature rise will be infinitesimally small and so we can take it to be zero.

$$T_l(r,z)\Big|_{r\to\infty} - T_a = 0. \tag{3.15}$$

3.1.2 Steady state analysis

Consider Equation 3.9, at steady state. The term $\partial T/\partial t$ will be zero and Equation 3.9 will reduce to Equation 3.16.

$$\nabla_o T_l + \frac{\partial^2 T_l}{\partial z^2} = 0. \tag{3.16}$$

We will be using the novel Hankel transform to solve the partial differential equation (PDE).

Hankel Transform

Hankel transform is an integral transform analogous to a 2D Fourier transform of radially symmetric functions. It is also known as Fourier-Bessel transform [24, 25]. The zero order Hankel transform is given in Equation 3.17.

$$\overline{f}(\sigma) = \mathscr{H}_o\{f(r)\} = \int_0^\infty r f(r) J_o(\sigma r) dr, \tag{3.17}$$

where $\mathscr{H}_o$ represents the zero order Hankel transform, J_o is the zero order Bessel function of the first kind, r is in cylindrical co-ordinates, and σ is the Hankel domain variable.

Inverse Hankel transform is given by Equation 3.18

$$f(r) = \mathscr{H}_o^{-1}\{f(\sigma)\} = \int_0^\infty \sigma \overline{f}(\sigma) J_o(\sigma r) d\sigma. \tag{3.18}$$

Properties of Hankel transform used:

1. **Property 1:** For an arbitrary function $f(r)$ if $\lim_{r\to\infty} f(r) = 0$, the zero order Hankel transform of $\nabla_o f(r)$ is given by:

$$\mathscr{H}_o\left\{\nabla_o f(r)\right\} = -\sigma^2 \mathscr{H}_o\left\{f(r)\right\} = -\sigma^2 \overline{f}(\sigma), \tag{3.19}$$

   where ∇_o is the zero order Bessel differential operator defined in Equation 3.8

2. **Property 2:** The zero order Hankel transform of a step function $G(r)$ is given by Equation 3.21, where function $G(r)$ is given in Equation 3.20.

$$G(r) = \begin{cases} 1, & \text{for } |r| \leq r_o, \\ 0, & \text{otherwise.} \end{cases} \tag{3.20}$$

   Zero order Hankel transform of Equation 3.20 is given in Equation 3.21.

$$\mathscr{H}_o\left\{G(r)\right\} = \frac{r_o J_1(r_o \sigma)}{\sigma}. \tag{3.21}$$

Solution

We are interested in the temperature rise with respect to the ambient temperature (T_a). So let us subtract the ambient temperature from $T_l(r, z)$ and set it up equal to $\phi_l(r, z)$.

$$\phi_l(r, z) = T_l(r, z) - T_a. \tag{3.22}$$

Putting $\phi_l(r, z)$ into Equation 3.16, we will get:

$$\nabla_o \phi_l(r, z) + \frac{\partial^2}{\partial z^2}\phi_l(r, z) = 0. \tag{3.23}$$

We compute the Hankel transform of both side of Equation 3.23, we will get:

$$\mathscr{H}_o\left\{\nabla_o \phi_l(r, z)\right\} + \frac{\partial^2}{\partial z^2}\mathscr{H}_o\{\phi_l(r, z)\} = 0. \tag{3.24}$$

Using the property of the Hankel transform given in Equation 3.19, we will get:

$$-\sigma^2 \mathscr{H}_o\ \{\phi_l(r,z)\} + \frac{\partial^2}{\partial z^2}\mathscr{H}_o\{\phi_l(r,z)\} = 0, \tag{3.25}$$

$$\frac{\partial^2 \overline{\phi_l}}{\partial z^2} = \sigma^2 \overline{\phi_l}. \tag{3.26}$$

where $\overline{\ }$ represents the Hankel transform. Equation 3.26 is an ordinary differential equation (ODE), whose general solution for the:

1. Temperature profile of the silicon die is:

$$\overline{\phi_1} = C_1 e^{\sigma z} + C_2 e^{-\sigma z}. \tag{3.27}$$

2. Temperature profile of the heat spreader is:

$$\overline{\phi_2} = C_3 e^{\sigma z} + C_4 e^{-\sigma z}. \tag{3.28}$$

Hankel transform of boundary conditions We compute the zero order Hankel transform of the boundary conditions and apply them to Equation 3.27 and Equation 3.28.

1. First boundary condition:

$$-k_1 \frac{\partial T_1}{\partial z}\bigg|_{z=0} = \begin{cases} q_o, & \text{for } |r| \le r_o, \\ 0, & \text{otherwise.} \end{cases} \tag{3.29}$$

Putting $\phi_l(r,z)$ into Equation 3.29, we will get:

$$-k_1 \frac{\partial \phi_1(r,z)}{\partial z}\bigg|_{z=0} = \begin{cases} q_o, & \text{for } |r| \le r_o, \\ 0, & \text{otherwise.} \end{cases} \tag{3.30}$$

Taking the Hankel transform of both side of Equation 3.30 and using the property of the Hankel transform given in Equation 3.21

$$-k_1 \frac{\partial \overline{\phi_1}}{\partial z}\bigg|_{z=0} = q_o r_o \frac{J_1(r_o\sigma)}{\sigma}. \tag{3.31}$$

Putting Equation 3.27 into Equation 3.31 and solving, we will get:

$$-k_1 \frac{\partial}{\partial z}\Big(C_1 e^{\sigma z} + C_2 e^{-\sigma z}\Big)\bigg|_{z=0} = q_o r_o \frac{J_1(r_o\sigma)}{\sigma}, \tag{3.32}$$

$$-k_1 \sigma\Big(C_1 e^{\sigma z} - C_2 e^{-\sigma z}\Big)\bigg|_{z=0} = q_o r_o \frac{J_1(r_o\sigma)}{\sigma}, \tag{3.33}$$

$$\boxed{C_2 - C_1 = \frac{q_o r_o}{k_1}\frac{J_1(r_o\sigma)}{\sigma^2}.} \tag{3.34}$$

2. Second boundary condition:

$$-k_1\frac{\partial T_1}{\partial z}\Big|_{z=\delta} = -k_2\frac{\partial T_2}{\partial z}\Big|_{z=\delta}. \tag{3.35}$$

Putting $\phi_l(r,z)$ into Equation 3.35, we will get:

$$-k_1\frac{\partial \phi_1}{\partial z}\Big|_{z=\delta} = -k_2\frac{\partial \phi_2}{\partial z}\Big|_{z=\delta}. \tag{3.36}$$

Taking the Hankel tranform of both sides, we will get:

$$-k_1\frac{\partial \overline{\phi_1}}{\partial z}\Big|_{z=\delta} = -k_2\frac{\partial \overline{\phi_2}}{\partial z}\Big|_{z=\delta}. \tag{3.37}$$

Putting Equation 3.28 and Equation 3.27 into Equation 3.37, we will get:

$$-k_1\frac{\partial}{\partial z}\Big(C_1e^{\sigma z}+C_2e^{-\sigma z}\Big)\Big|_{z=\delta} = -k_2\frac{\partial}{\partial z}\Big(C_3e^{\sigma z}+C_4e^{-\sigma z}\Big)\Big|_{z=\delta}, \tag{3.38}$$

$$\sigma k_1\Big(C_1e^{\sigma z}-C_2e^{-\sigma z}\Big)\Big|_{z=\delta} = \sigma k_2\Big(C_3e^{\sigma z}-C_4e^{-\sigma z}\Big)\Big|_{z=\delta}, \tag{3.39}$$

$$\boxed{\frac{k_1}{k_2}\Big(\ C_1e^{\sigma\delta}-C_2e^{-\sigma\delta}\ \Big)-C_3e^{\sigma\delta}+C_4e^{-\sigma\delta}=0.} \tag{3.40}$$

3. Third boundary condition:

$$T_1(r,z)\Big|_{z=\delta} = T_2(r,z)\Big|_{z=\delta}. \tag{3.41}$$

Putting $\phi_l(r,z)$ into Equation 3.41, we will get:

$$\phi_1(r,z)\Big|_{z=\delta} = \phi_2(r,z)\Big|_{z=\delta}. \tag{3.42}$$

Taking the Hankel tranform of both sides, we will get:

$$\overline{\phi_1}(\sigma,z)\Big|_{z=\delta} = \overline{\phi_2}(\sigma,z)\Big|_{z=\delta}. \tag{3.43}$$

Putting Equation 3.28 and Equation 3.27 into Equation 3.44, we will get:

$$\Big(C_1e^{\sigma z}+C_2e^{-\sigma z}\Big)\Big|_{z=\delta} = \Big(C_3e^{\sigma z}+C_4e^{-\sigma z}\Big)\Big|_{z=\delta}. \tag{3.44}$$

$$\boxed{C_1e^{\sigma\delta}+C_2e^{-\sigma\delta}-C_3e^{\sigma\delta}-C_4e^{-\sigma\delta}=0.} \tag{3.45}$$

4. Fourth boundary condition:

$$T_2(r,z)\Big|_{z=\delta+b} = T_a. \tag{3.46}$$

Putting $\phi_l(r,z)$ into Equation 3.46, we will get:

$$\phi_2(r,z)\Big|_{z=\delta+b} = 0. \tag{3.47}$$

Taking the Hankel tranform of both sides, we will get:

$$\overline{\phi_2}(\sigma,z)\Big|_{z=\delta+b} = 0. \tag{3.48}$$

Putting Equation 3.28 and Equation 3.27 into Equation 3.49, we will get:

$$\Big(C_3e^{\sigma z} + C_4e^{-\sigma z}\Big)\Big|_{z=\delta+b} = 0. \tag{3.49}$$

$$\boxed{C_3 = -C_4e^{-2\sigma(\delta+b)}.} \tag{3.50}$$

Putting the value of C_3 in Equation 3.40, we will get:

$$\frac{k_1}{k_2}\Big(\ C_1e^{\sigma\delta} - C_2e^{-\sigma\delta}\ \Big) + C_4\Big(e^{-\sigma\delta} + e^{-\sigma\delta-2b\sigma}\Big) = 0, \tag{3.51}$$

Putting the value of C_3 in Equation 3.45, we will get:

$$C_1e^{\sigma\delta} + C_2e^{-\sigma\delta} = C_4\Big(e^{-\sigma\delta} - e^{-\sigma\delta-2b\sigma}\Big). \tag{3.52}$$

$$C_4 = \frac{C_1e^{\sigma\delta} + C_2e^{-\sigma\delta}}{e^{-\sigma\delta} - e^{-\sigma\delta-2b\sigma}}. \tag{3.53}$$

Putting the value of C_4 in Equation 3.51, we will get:

$$\frac{k_1}{k_2}\Big(\ C_1e^{\sigma\delta} - C_2e^{-\sigma\delta}\ \Big) = -\frac{e^{-\sigma\delta} + e^{-\sigma\delta-2b\sigma}}{e^{-\sigma\delta} - e^{-\sigma\delta-2b\sigma}}\Big(C_1e^{\sigma\delta} + C_2e^{-\sigma\delta}\Big), \tag{3.54}$$

$$\frac{C_2e^{-\sigma\delta} + C_1e^{\sigma\delta}}{C_2e^{-\sigma\delta} - C_1e^{\sigma\delta}} = \frac{k_1}{k_2}\left(\ \frac{e^{-\sigma\delta} - e^{-\sigma\delta-2b\sigma}}{e^{-\sigma\delta} + e^{-\sigma\delta-2b\sigma}}\ \right), \tag{3.55}$$

$$\frac{C_2e^{-\sigma\delta} + C_1e^{\sigma\delta}}{C_2e^{-\sigma\delta} - C_1e^{\sigma\delta}} = \frac{k_1}{k_2}\underbrace{\left(\ \frac{e^{b\sigma} - e^{-b\sigma}}{e^{b\sigma} + e^{-b\sigma}}\ \right)}_{\tanh(b\sigma)}, \tag{3.56}$$

$$\frac{C_2}{C_1}e^{-2\sigma\delta} = \frac{k_1\tanh(b\sigma) + k_2}{k_1\tanh(b\sigma) - k_2}, \tag{3.57}$$

$$C_1 = C_2 \underbrace{e^{-2\sigma\delta}\left(\frac{k_1\tanh(b\sigma)-k_2}{k_1\tanh(b\sigma)+k_2}\right)}_{f(\sigma)}, \tag{3.58}$$

$$C_1 = C_2 f(\sigma). \tag{3.59}$$

Putting the value of C_1 into Equation 3.34. We will get the value of desired constants C_1 and C_2.

$$C_1 = \frac{q_o r_o}{k_1}\frac{J_1(r_o\sigma)}{\sigma^2}\frac{f(\sigma)}{1-f(\sigma)}, \tag{3.60}$$

$$C_2 = \frac{q_o r_o}{k_1}\frac{J_1(r_o\sigma)}{\sigma^2}\frac{1}{1-f(\sigma)}, \tag{3.61}$$

where $f(\sigma)$ is defined in Equation 3.62

$$f(\sigma) = e^{-2\sigma\delta}\frac{k_1\tanh(b\sigma)-k_2}{k_1\tanh(b\sigma)+k_2}. \tag{3.62}$$

Putting the value of constants C_1 and C_2 into Equation 3.27. We will get the equation of the desired temperature profile in Hankel domain i.e. Temperature distributing function of the silicon die in Hankel domain.

$$\overline{\phi}_1(\sigma,z) = \frac{q_o r_o}{k_1}\frac{J_1(r_o\sigma)}{\sigma^2}\frac{1}{1-f(\sigma)}\Big(e^{-\sigma z}+f(\sigma)e^{\sigma z}\Big). \tag{3.63}$$

Temperature profile of the silicon die in cylindrical co-ordinates is given in Equation 3.64.

$$\boxed{T_1(r,z)-T_a = \frac{q_o r_o}{k_1}\int_0^\infty \frac{J_1(r_o\sigma)}{\sigma}\frac{(e^{-\sigma z}+f(\sigma)e^{\sigma z})}{1-f(\sigma)}J_o(\sigma r)d\sigma} \tag{3.64}$$

Analytical verification

Let us verify the obtained solution using the fifth and sixth boundary conditions (see Equation 3.14 and 3.15).

1. **Fifth boundary condition:** We will only verify for the temperature distribution of the silicon die ($T_1(r,z)$). For the silicon die the fifth boundary is given in Equation 3.65

$$-k_1\frac{\partial T_1}{\partial r}\Big|_{r=0} = 0. \tag{3.65}$$

Putting the obtained result (Equation 3.64) into Equation 3.65. We will get:

$$-k_1\frac{\partial T_1}{\partial r}\Big|_{r=0} = -k_1\frac{\partial}{\partial r}\left(\frac{q_o r_o}{k_1}\int_0^\infty \frac{J_1(r_o\sigma)}{\sigma}\frac{(e^{-\sigma z}+f(\sigma)e^{\sigma z})}{1-f(\sigma)}J_o(\sigma r)d\sigma\right)\Big|_{r=0}. \quad (3.66)$$

Using the Leibniz integral rule [26] to solve Equation 3.66. The Leibniz integral rule is given in Equation 3.67.

$$\frac{d}{dx}\int_{a(x)}^{b(x)} f(x,t)dt = f(x,b(x)).b'(x) - f(x,a(x)).a'(x) + \int_{a(x)}^{b(x)}\frac{d}{dx}f(x,t)dt. \quad (3.67)$$

Equation 3.66 will reduce to Equation 3.68.

$$= \frac{q_o r_o}{k_1}\int_0^\infty \frac{J_1(r_o\sigma)}{\sigma}\frac{(e^{-\sigma z}+f(\sigma)e^{\sigma z})}{1-f(\sigma)}J_1(\sigma r)d\sigma\Big|_{r=0}, \quad (3.68)$$

$$= \frac{q_o r_o}{k_1}\int_0^\infty \frac{J_1(r_o\sigma)}{\sigma}\frac{(e^{-\sigma z}+f(\sigma)e^{\sigma z})}{1-f(\sigma)}J_1(0)d\sigma \quad (3.69)$$

Hence, we will get:

$$-k_1\frac{\partial T_1}{\partial r}\Big|_{r=0} = 0. \quad (3.70)$$

2. **Sixth boundary condition:** Let us re-write Equation 3.15, we will get Equation 3.71

$$\lim_{r\to\infty}\Big(T(r,z)-T_a\Big) = \lim_{r\to\infty}\phi(r,z) = 0. \quad (3.71)$$

Putting the obtained result (Equation 3.64) into Equation 3.71. We will get:

$$\begin{aligned}\lim_{r\to\infty}\Big(T_1(r,z)-T_a\Big) &= \lim_{r\to\infty}\phi(r,z)\\ &= \lim_{r\to\infty}\frac{q_o r_o}{k_1}\int_0^\infty \frac{J_1(r_o\sigma)}{\sigma}\frac{(e^{-\sigma z}+f(\sigma)e^{\sigma z})}{1-f(\sigma)}J_o(\sigma r)d\sigma,\end{aligned} \quad (3.72)$$

$$= \frac{q_o r_o}{k_1}\int_0^\infty \frac{J_1(r_o\sigma)}{\sigma}\frac{(e^{-\sigma z}+f(\sigma)e^{\sigma z})}{1-f(\sigma)}\lim_{r\to\infty}\left(J_o(\sigma r)\right)d\sigma, \quad (3.73)$$

$$= \frac{q_o r_o}{k_1}\int_0^\infty \frac{J_1(r_o\sigma)}{\sigma}\frac{(e^{-\sigma z}+f(\sigma)e^{\sigma z})}{1-f(\sigma)}J_o(\infty)d\sigma, \quad (3.74)$$

Hence, we will get:

$$\lim_{r\to\infty} T(r,z) - T_a = 0. \quad (3.75)$$

3.1.3 Transient analysis

Consider the transient Fourier heat equation given in Equation 3.9.

$$-\frac{\rho_l c_l}{k_l}\left(\frac{\partial T_l}{\partial t}\right) + \nabla_o T_l + \frac{\partial^2 T_l}{\partial z^2} = 0. \quad (3.76)$$

We will be using the Laplace transform to remove the time derivative and after that the Hankel transform similar to the Fourier steady state analysis (see section 3.1.2).

Laplace Transform

Laplace transform is an integral transform, it is a very useful tool for solving differential equations. Unlike Fourier transform which is a complex function of a real variable (frequency), Laplace transform is a complex function of a complex variable [24]. The Laplace transform is given in Equation 3.77.

$$\mathscr{L}\{f(t)\} = \boldsymbol{F}(s) = \int_{-\infty}^{\infty} f(t)e^{-st}dt, \tag{3.77}$$

where s is a complex Laplace domain variable.

Inverse Laplace transform also known as the Mellin's inverse, Fourier-Mellin integral, or Bromwich integral is given in Equation 3.78 [24, 27].

$$f(t) = \mathscr{L}^{-1}\{\boldsymbol{F}(s)\} = \frac{1}{2\pi i}\int_{\gamma-i\infty}^{\gamma+i\infty} e^{st}\boldsymbol{F}(s)ds, \tag{3.78}$$

where $Re(s) = \gamma$ is a vertical contour in the complex plain such the all the singularities of $\boldsymbol{F}(s)$ are to the left of it.

Property of the Laplace transform used:

1. **Property 1:** Laplace transform of a derivative of a function $f(t)$ is given by:

$$\mathscr{L}\left\{\frac{d}{dt}f(t)\right\} = s\boldsymbol{F}(s). \tag{3.79}$$

Solution

We are interested in the temperature rise with respect to the ambient temperature (T_a). So let us subtract the ambient temperature from $T_l(t, r, z)$ and set it up equal to $\phi_l(t, r, z)$.

$$\phi_l(r, z, t) = T_l(r, z, t) - T_a. \tag{3.80}$$

Putting the value of ϕ_l into Equation 3.76

$$-\frac{\rho_l c_l}{k_l}\left(\frac{\partial}{\partial t}\phi_l(r, z, t)\right) + \nabla_o\phi_l(r, z, t) + \frac{\partial^2}{\partial z^2}\phi_l(r, z, t) = 0. \tag{3.81}$$

Compute the Laplace transform of both side of the Equation 3.81 such that the system was at rest for $t \leq 0$ and using the property of the Laplace transform given in Equation 3.79, we will get Equation 3.82.

$$-s\frac{\rho_l c_l}{k_l}\boldsymbol{\phi_l} + \nabla_o \boldsymbol{\phi_l} + \frac{\partial^2}{\partial z^2}\boldsymbol{\phi_l} = 0. \tag{3.82}$$

Here, $\boldsymbol{\phi}$ represents the Laplace transform. Compute the Hankel transform similar to steady state analysis (see section 3.1.2).

$$-s\frac{\rho_l c_l}{k_l}\mathscr{H}_o\{\boldsymbol{\phi_l}\} + \mathscr{H}_o\{\nabla_o \boldsymbol{\phi_l}\} + \frac{\partial^2}{\partial z^2}\mathscr{H}_o\{\boldsymbol{\phi_l}\} = 0. \tag{3.83}$$

$$-s\frac{\rho_l c_l}{k_l}\overline{\boldsymbol{\phi_l}} - \sigma^2\overline{\boldsymbol{\phi_l}} + \frac{\partial^2}{\partial z^2}\overline{\boldsymbol{\phi_l}} = 0. \tag{3.84}$$

After re-arrangement, we will get Equation 3.85.

$$\frac{\partial^2}{\partial z^2}\overline{\boldsymbol{\phi_l}} = \left(\sigma^2 + s\frac{\rho_l c_l}{k_l}\right)\overline{\boldsymbol{\phi_l}}. \tag{3.85}$$

Equation 3.85 is an ODE, whose general solution for the:

1. Temperature profile of the silicon die is:

$$\overline{\boldsymbol{\phi_1}} = C_5 e^{p_1(s,\sigma)z} + C_6 e^{-p_1(s,\sigma)z}. \tag{3.86}$$

2. Temperature profile of the heat spreader is:

$$\overline{\boldsymbol{\phi_2}} = C_7 e^{p_2(s,\sigma)z} + C_8 e^{-p_2(s,\sigma)z}, \tag{3.87}$$

where $p_l(s,z)$ is given in Equation 3.88.

$$p_l(s,\sigma) = \sqrt{\sigma^2 + \frac{\rho_l c_l}{k_l}s}. \tag{3.88}$$

Hankel transform and Laplace of boundary conditions We compute the Laplace and zero order Hankel transform of the boundary conditions and apply them to Equation 3.27 and Equation 3.28.

1. First boundary condition:

$$-k_1\left.\frac{\partial T_1}{\partial z}\right|_{z=0} = \begin{cases} q_o u(t), & \text{for } |r| \leq r_o, \\ 0, & \text{otherwise.} \end{cases} \tag{3.89}$$

where $u(t)$ is the unit step response. Putting $\phi_l(t,r,z)$ into Equation 3.89, we will get:

$$-k_1\frac{\partial\phi_1(t,r,z)}{\partial z}\bigg|_{z=0} = \begin{cases} q_o u(t), & \text{for } |r| \le r_o, \\ 0, & \text{otherwise.} \end{cases} \tag{3.90}$$

Taking the Laplace transform of both side of Equation 3.90, we will get:

$$-k_1\frac{\partial\boldsymbol{\phi_1}}{\partial z}\bigg|_{z=0} = \begin{cases} \frac{q_o}{s}, & \text{for } |r| \le r_o, \\ 0, & \text{otherwise.} \end{cases} \tag{3.91}$$

Taking the Hankel transform of both side of Equation 3.91 and using the property of the Hankel transform given in Equation 3.21

$$-k_1\frac{\partial\overline{\phi_1}}{\partial z}\bigg|_{z=0} = q_o r_o\frac{J_1(r_o\sigma)}{s\sigma}. \tag{3.92}$$

Putting Equation 3.86 into Equation 3.92 and solving, we will get:

$$-k_1\frac{\partial}{\partial z}\Big(C_5e^{p_1(s,\sigma)z} + C_6e^{-p_1(s,\sigma)z}\Big)\bigg|_{z=0} = q_o r_o\frac{J_1(r_o\sigma)}{s\sigma}, \tag{3.93}$$

$$-k_1p_1(s,\sigma)\Big(C_5e^{p_1(s,\sigma)z} - C_6e^{-p_1(s,\sigma)z}\Big)\bigg|_{z=0} = q_o r_o\frac{J_1(r_o\sigma)}{s\sigma}, \tag{3.94}$$

$$\boxed{C_6 - C_5 = \frac{q_o r_o}{k_1}\frac{J_1(r_o\sigma)}{p_1(s,\sigma)s\sigma}.} \tag{3.95}$$

2. Second boundary condition:

$$-k_1\frac{\partial T_1}{\partial z}\Big|_{z=\delta} = -k_2\frac{\partial T_2}{\partial z}\Big|_{z=\delta}. \tag{3.96}$$

Putting $\phi_l(t,r,z)$ into Equation 3.35, we will get:

$$-k_1\frac{\partial\phi_1}{\partial z}\Big|_{z=\delta} = -k_2\frac{\partial\phi_2}{\partial z}\Big|_{z=\delta}. \tag{3.97}$$

Taking the Laplace and Hankel tranform of both side, we will get:

$$-k_1\frac{\partial\overline{\boldsymbol{\phi_1}}}{\partial z}\Big|_{z=\delta} = -k_2\frac{\partial\overline{\boldsymbol{\phi_1}}}{\partial z}\Big|_{z=\delta}. \tag{3.98}$$

Putting Equation 3.87 and Equation 3.86 into Equation 3.98, we will get:

$$-k_1\frac{\partial}{\partial z}\Big(C_5e^{p_1(s,\sigma)z} + C_6e^{-p_1(s,\sigma)z}\Big)\bigg|_{z=\delta} = -k_2\frac{\partial}{\partial z}\Big(C_7e^{p_2(s,\sigma)z} + C_8e^{-p_2(s,\sigma)z}\Big)\bigg|_{z=\delta}, \tag{3.99}$$

$$p_1(s,\sigma)k_1\Big(C_5e^{p_1(s,\sigma)z} - C_6e^{-p_1(s,\sigma)z}\Big)\Big|_{z=\delta} = p_2(s,\sigma)k_2\Big(C_7e^{p_2(s,\sigma)z} - C_8e^{-p_2(s,\sigma)z}\Big)\Big|_{z=\delta}, \tag{3.100}$$

$$\boxed{\frac{k_1p_1(s,\sigma)}{k_2p_2(s,\sigma)}\Big(\ C_5e^{p_1(s,\sigma)\delta} - C_6e^{-p_1(s,\sigma)\delta}\ \Big) - C_7e^{p_2(s,\sigma)\delta} + C_8e^{-p_2(s,\sigma)\delta} = 0.} \tag{3.101}$$

3. Third boundary condition:

$$T_1(t,r,z)\Big|_{z=\delta} = T_2(t,r,z)\Big|_{z=\delta}. \tag{3.102}$$

Putting $\phi_l(t,r,z)$ into Equation 3.102, we will get:

$$\phi_1(t,r,z)\Big|_{z=\delta} = \phi_2(t,r,z)\Big|_{z=\delta}. \tag{3.103}$$

Taking the Laplace and Hankel tranform on both side, we will get:

$$\overline{\phi_1}(s,\sigma,z)\Big|_{z=\delta} = \overline{\phi_2}(s,\sigma,z)\Big|_{z=\delta}. \tag{3.104}$$

Putting Equation 3.87 and Equation 3.86 into Equation 3.104, we will get:

$$\Big(C_5e^{p_1(s,\sigma)z} - C_6e^{-p_1(s,\sigma)z}\Big)\Big|_{z=\delta} = \Big(C_7e^{p_2(s,\sigma)z} - C_8e^{-p_2(s,\sigma)z}\Big)\Big|_{z=\delta}. \tag{3.105}$$

$$\boxed{C_5e^{p_1(s,\sigma)\delta} + C_6e^{-p_1(s,\sigma)\delta} - C_7e^{p_2(s,\sigma)\delta} - C_8e^{-p_2(s,\sigma)\delta} = 0.} \tag{3.106}$$

4. Fourth boundary condition:

$$T_2(t,r,z)\Big|_{z=\delta+b} = T_a. \tag{3.107}$$

Putting $\phi_l(r,z)$ into Equation 3.107, we will get:

$$\phi_2(t,r,z)\Big|_{z=\delta+b} = 0. \tag{3.108}$$

Taking the Laplace and Hankel transform of both side, we will get:

$$\overline{\phi_2}(s,\sigma,z)\Big|_{z=\delta+b} = 0. \tag{3.109}$$

Putting Equation 3.87 and Equation 3.86 into Equation 3.109, we will get:

$$\Big(C_7e^{p_2(s,\sigma)z} + C_8e^{-p_2(s,\sigma)z}\Big)\Big|_{z=\delta+b} = 0. \tag{3.110}$$

$$\boxed{C_7 = -C_8e^{-2p_2(s,\sigma)(\delta+b)}.} \tag{3.111}$$

On solving using elimination method, we will get the desired value of constants C_5 and

C_6.

$$C_5 = \frac{q_o r_o}{k_1} \frac{J_1(r_o\sigma)}{p_1(s,\sigma)s\sigma} \frac{f(s,\sigma)}{1-f(s,\sigma)}, \tag{3.112}$$

$$C_6 = \frac{q_o r_o}{k_1} \frac{J_1(r_o\sigma)}{p_1(s,\sigma)s\sigma} \frac{1}{1-f(s,\sigma)}, \tag{3.113}$$

where $f(s,\sigma)$ is given in Equation 3.114

$$f(s,\sigma) = e^{-2p_1(s,\sigma)\delta} \frac{k_1 p_1(s,\sigma)\tanh(p_2(s,\sigma)b) - k_2 p_2(s,\sigma)}{k_1 p_1(s,\sigma)\tanh(p_2(s,\sigma)b) + k_2 p_2(s,\sigma)}. \tag{3.114}$$

Putting the value of constant C_5 and C_6 into Equation 3.86. We will get the Equation of desired temperature profile in Laplace and Hankel domain i.e. Temperature distribution function of the silicon die in Laplace and Hankel domain.

$$\boxed{\overline{\phi_1}(\sigma,z,s) = \frac{q_o r_o}{k_1} \frac{J_1(r_o\sigma)}{p_1(s,\sigma)s\sigma} \frac{1}{1-f(s,\sigma)} \left(e^{-p_1(s,\sigma)z} + f(s,\sigma)e^{p_1(s,\sigma)z}\right)} \tag{3.115}$$

The temperature of the silicon die in time domain and cylindrical co-ordinates can be calculated using the simple inverse Laplace and Hankel transforms respectively.

$$T_1(r,z,t) - T_a = \mathscr{H}^{-1}\{\mathscr{L}^{-1}\{\overline{\phi_1}(\sigma,z,s)\}\}. \tag{3.116}$$

Analytical verification

Let us verify the obtained solution using the final value theorem and see if it converges to steady state solution. Final value theorem is defined in Equation 3.117.

$$\lim_{t\to\infty} f(t) = \lim_{s\to 0} sF(s). \tag{3.117}$$

The relation given in Equation 3.117 is valid such that the $f(t)$ is bounded on $(0,\infty)$. $F(s)$ is an unilateral Laplace transform of $f(t)$.

From the steady state solution we know:

$$\lim_{t\to\infty} f(t) = \frac{q_o r_o}{k_1} \frac{J_1(r_o\sigma)}{\sigma^2} \frac{1}{1-f(\sigma)} \left(e^{-\sigma z} + f(\sigma)e^{\sigma z}\right). \tag{3.118}$$

Let us compute $\lim_{s\to 0} sF(s)$ by putting Equation 3.115 into 3.117.

$$\lim_{s\to 0} sF(s) = \lim_{s\to 0} s\frac{q_o r_o}{k_1} \frac{J_1(r_o\sigma)}{p_1(s,\sigma)s\sigma} \frac{1}{1-f(s,\sigma)} \left(e^{-p_1(s,\sigma)z} + f(s,\sigma)e^{p_1(s,\sigma)z}\right) \tag{3.119}$$

$$= \lim_{s\to 0} \frac{q_o r_o}{k_1} \frac{J_1(r_o\sigma)}{p_1(s,\sigma)\sigma} \frac{1}{1-f(s,\sigma)} \left(e^{-p_1(s,\sigma)z} + f(s,\sigma)e^{p_1(s,\sigma)z}\right) \tag{3.120}$$

$$= \frac{q_o r_o}{k_1} \frac{J_1(r_o\sigma)}{p_1(0,\sigma)\sigma} \frac{1}{1-f(0,\sigma)} \left(e^{-p_1(0,\sigma)z} + f(0,\sigma) e^{p_1(0,\sigma)z} \right) \tag{3.121}$$

$$= \frac{q_o r_o}{k_1} \frac{J_1(r_o\sigma)}{\sigma^2} \frac{1}{1-f(\sigma)} \left(e^{-\sigma z} + f(\sigma) e^{\sigma z} \right) \tag{3.122}$$

$$= \lim_{t\to\infty} f(t) \tag{3.123}$$

Transient Fourier solution converges to steady state Fourier solution.

3.1.4 Correction for Edges and Corners

The size of the chip is finite; however, for simplicity, we assume it to be infinite. This assumption results in an error in the calculation of the Green's function at the edges and the corners. To overcome this problem, we calculate the Green's function beyond the boundary of the chip (extended Green's function). This extended Green's function is then convolved with the power profile to obtain an extended thermal profile. The profile is then folded across the corners and edges to get the corrected thermal profile, since the boundaries are adiabatic.

3.2 Boltzmann transport equation

The classical continuum Fourier heat equation fails to predict the temperature profile when the device characteristic length is comparable to mean free path of heat carriers as the Fourier heat equation does not take into account the effects of phonon scattering [13, 20, 14, 15]. Different models have been developed to model heat transport at the nanoscale level like Molecular dynamics method, Ballistic method, and Boltzmann transport equation. Molecular dynamics model is a computationally intensive method, and it can not be applied to a very large system like a FET, Ballistic equation is computationally less intensive, but it does not provide an adequate accuracy. BTE is computationally less intensive and provides acceptable accuracy [13, 16]. The mathematical formulation of BTE is given in Equation 3.124 [13, 14].

$$\frac{\partial e_\omega}{\partial t} + \nabla . \vec{\boldsymbol{s}} v_g e_\omega - \frac{Q_\omega}{4\pi} = S_{scattering}, \tag{3.124}$$

where $e_\omega(\omega, \boldsymbol{r}, \vec{\boldsymbol{s}}, t)$ is the energy density per unit solid angle and it is a function of $\omega, \boldsymbol{r}, \vec{\boldsymbol{s}}$ and t. The space vector $\boldsymbol{r}$ has three components (x,y and z are in cartesian co-ordinates), the direction of momentum $\vec{\boldsymbol{s}}$ has two components, the oplar angle θ and azimulthal angle ϕ, ω is the phonon frequency, and t is the time. The subscript ω represents dependence on the frequency. v_g is the phonon group velocity [13, 14, 28, 29], and the term on the right-hand side of Equation 3.124 is the scattering term. It models the phonon scattering, collision

with other phonons, and impurities. This term makes the solution of the BTE complex, for simplification we will use the Bhatnagar–Gross–Krook model [**?** 13, 14, 28, 29].

$$\frac{\partial e_\omega}{\partial t} + \nabla.\vec{\boldsymbol{s}} v_g e_\omega - \frac{Q_\omega}{4\pi} = -\frac{e_w - e_o(T)}{\tau}, \tag{3.125}$$

where $e_o(T)$ is the equilibrium energy density, τ is the phonon relaxation time, and Q_ω is

Table 3.2: Glossary

Symbol	Full Form	Meaning
e_ω	$e_\omega(\omega, \boldsymbol{r}, \vec{\boldsymbol{s}}, t)$	Energy density per unit solid angle
e	$e(\boldsymbol{r}, \vec{\boldsymbol{s}}, t)$	Frequency independent energy density per unit solid angle
e_o	$e(T)$	Equilibrium energy density
v_g		Group velocity
ω		Frequency
Ω		Solid angle
$\vec{\boldsymbol{s}}$		Direction vector
$\sim$	overtilde	Fourier Transform

the volumetric heat generation. The term $\nabla.\vec{\boldsymbol{s}} v_g e_w$ will expand into Equation 3.126 [20, 28, 14, 13].

$$\nabla.\vec{\boldsymbol{s}} v_g = v_g \cos\theta \frac{\partial e_\omega}{\partial z} + v_g \sin\theta \cos\phi \frac{\partial e_\omega}{\partial x} + v_g \sin\theta \sin\phi \frac{\partial e_\omega}{\partial y}, \tag{3.126}$$

where θ and ϕ are polar and azimuthal angles respectively. To further simplify the BTE (Equation 3.125), we will use the gray model of BTE. Gray BTE assumes that all phonons are tied to a single mode, means all phonons have the same group velocity and the relaxation time. This approach is faster than the frequency dependent (multi-mode) BTE and gives reasonable accuracy [15]. Gray BTE is given in Equation 3.129.

$$\frac{\partial e}{\partial t} + \nabla.\vec{\boldsymbol{s}} v_g e - \frac{Q}{4\pi} = -\frac{e - e_o(T)}{\tau}. \tag{3.127}$$

For a small temperature rise, $\Delta T = T - T_{ref}$. The relation between T and $e_o(T)$ is given in Equation 3.128 [20, 14, 13].

$$e_o(T) = \frac{1}{4\pi} C \Delta T, \tag{3.128}$$

where C is the specific heat at the reference temperature, T_{ref} is the reference temperature (computed by Fourier analysis), and T is the lattice temperature.

We are interested in computing the temperature rise (ΔT) but we have two unknowns terms in the gray BTE: 1) Temperature rise (ΔT) 2) Energy density per unit solid angle

(e). To find a closed form solution, we need a relation between the temperature rise and the energy density per unit solid angle. Let us integrate the gray BTE over the solid angle (Ω) of both sides of Equation 3.129. We will get:

$$\frac{\partial}{\partial t}\underbrace{\int e\,d\Omega}_{\substack{\text{System}\\ \text{energy per}\\ \text{unit volme}}} + \nabla.\underbrace{\int \vec{\boldsymbol{s}} v_g e\,d\Omega}_{\text{Heat flux}} - \underbrace{\int \frac{Q}{4\pi}\,d\Omega}_{\substack{\text{Heat}\\ \text{generation}}} = -\int \frac{e - e_o(T)}{\tau}\,d\Omega \tag{3.129}$$

The left hand side of Equation 3.129 will convert to a well known form given in Equation 3.130 [30].

$$\frac{\partial E}{\partial t} + \nabla.q - Q, \tag{3.130}$$

where $E = \int e\,d\Omega$ is the system energy per unit volume, $q = \int \vec{\boldsymbol{s}} v_g e\,d\Omega$ is the heat flux, and $Q = \int Q/4\pi\,d\Omega$ is the volumetric heat generation. Equation 3.130 is the energy conservation equation, which will be equal to zero. Hence, the right hand side of Equation 3.129 (after integration) has to be zero. We will have:

$$\int_\Omega \left[\frac{e - e_o(T)}{\tau} \right] d\Omega = 0 \tag{3.131}$$

Putting the value of equilibrium energy density ($e_o(T)$). We thus have the desired relation:

$$\int_\Omega \left[\frac{e}{\tau} - \frac{1}{4\pi}\frac{C}{\tau}\Delta T \right] d\Omega = 0 \tag{3.132}$$

3.2.1 Steady state analysis

Consider the gray BTE (Equation 3.129), at steady state the term $\partial e/\partial t$ will be zero and Equation 3.129 will reduce to Equation 3.141.

$$\nabla.\vec{\boldsymbol{s}} v_g e - \frac{Q}{4\pi} = -\frac{e - e_o(T)}{\tau} \tag{3.133}$$

We will use the Fourier transform to solve the integro-differential equation.

Fourier Transform

Fourier transform is an integral transform. It decomposes a bounded function $f(x)$ defined over the infinite limits $(-\infty, \infty)$ into superimposition of sinusoid. One-dimensional Fourier

transform for a function $f(x)$ is given Equation 3.134

$$F(\xi) = \mathscr{F}\{f(x)\} = \int_{-\infty}^{\infty} f(x)e^{ix\xi}dx, \tag{3.134}$$

where $\mathscr{F}$ represents the Fourier transform, ξ is the Fourier domain variable (frequency), and i is equal to $\sqrt{-1}$.

Inverse Fourier transform is given in Equation 3.135

$$f(x) = \mathscr{F}^{-1}\{F(\xi)\} = \frac{1}{2\pi}\int_{-\infty}^{\infty} F(\xi)e^{ix\xi}d\xi. \tag{3.135}$$

***N*-Dimensions Fourier Transform** $N-$dimensional Fourier transform of a real or complex valued function $f(\vec{\boldsymbol{x}})$ of a vector variable $\vec{\boldsymbol{x}} = x_1, x_2, x_3, ..., x_N$ is given by:

$$F(\vec{\boldsymbol{\xi}}) = \mathscr{F}\{f(\vec{\boldsymbol{x}})\} = \int_{\boldsymbol{R^N}} f(\vec{\boldsymbol{x}})e^{-i\vec{\boldsymbol{x}}.\vec{\boldsymbol{\xi}}}d^N\vec{\boldsymbol{x}}, \tag{3.136}$$

where

$$\int_{\boldsymbol{R^N}} d^N\vec{\boldsymbol{x}} = \int_{-\infty}^{\infty} dx_1. \int_{-\infty}^{\infty} dx_2..... \int_{-\infty}^{\infty} dx_N, \tag{3.137}$$

$\vec{\boldsymbol{x}}$ and $\vec{\boldsymbol{\xi}}$ are vectors, $\boldsymbol{R}^N$ represents $N-$dimensional space. The term in the exponential is the dot product of $\vec{\boldsymbol{x}}$ and $\vec{\boldsymbol{\xi}}$ in $\boldsymbol{R}^N$ and it is given in Equation 3.138.

$$\vec{\boldsymbol{x}}.\vec{\boldsymbol{\xi}} = x_1\xi_1 + x_2\xi_2 + x_3\xi_3 + ... + x_{n-1}\xi_{n-1} + x_n\xi_N. \tag{3.138}$$

Inverse Fourier transform is given in Equation 3.139.

$$f(\vec{\boldsymbol{x}}) = \mathscr{F}^{-1}\{F(\vec{\boldsymbol{\xi}})\} = \frac{1}{(2\pi)^N}\int_{\boldsymbol{R^n}} F(\vec{\boldsymbol{\xi}})e^{i\vec{\boldsymbol{x}}.\vec{\boldsymbol{\xi}}}d^N\vec{\boldsymbol{\xi}}, \tag{3.139}$$

where

$$\int_{\boldsymbol{R^N}} d^N\vec{\boldsymbol{\xi}} = \int_{-\infty}^{\infty} d\xi_1. \int_{-\infty}^{\infty} d\xi_2..... \int_{-\infty}^{\infty} d\xi_N \tag{3.140}$$

Solution

Putting Equation 3.126 and 3.128 into the gray BTE (Equation 3.141). We will get:

$$v_g\cos\theta\frac{\partial e_\omega}{\partial z} + v_g\sin\theta\cos\phi\frac{\partial e_\omega}{\partial x} + v_g\sin\theta\sin\phi\frac{\partial e_\omega}{\partial y} - \frac{Q}{4\pi} = -\frac{e}{\tau} + \frac{1}{4\pi\tau}C\Delta T \tag{3.141}$$

Computing the Fourier transform of both sides. We will get:

$$(v_g \cos\theta i\xi_z + v_g \sin\theta \cos\phi i\xi_x + v_g \sin\theta \sin\phi i\xi_y)\widetilde{e} = -\frac{\widetilde{e}}{\tau} + \frac{C}{4\pi\tau}\Delta\widetilde{T} + \frac{\widetilde{Q}}{4\pi}, \tag{3.142}$$

where $\sim$ represents the Fourier transform, i is equal to $\sqrt{-1}$ and ξ_x, ξ_y and ξ_z are spatial frequency of x, y and z. Rearranging Equation 3.142, we will have:

$$\widetilde{e} = \frac{C}{4\pi}\frac{\Delta\widetilde{T} + \widetilde{Q}\tau/C}{1 + \Lambda\cos\theta i\xi_z + \Lambda\sin\theta\cos\phi i\xi_x + \Lambda\sin\theta\sin\phi i\xi_y}, \tag{3.143}$$

where Λ is the mean free path and it is equal to $v_g \times \tau$. Let us take the Fourier transform on both sides of Equation 3.144. We will get:

$$\int_\Omega \left[\frac{\widetilde{e}}{\tau} - \frac{1}{4\pi}\frac{C}{\tau}\Delta\widetilde{T} \right] d\Omega = 0 \tag{3.144}$$

Putting Equation 3.143 into Equation 3.132 and after rearranging we will get:

$$\Delta\widetilde{T} = \frac{1}{4\pi}\int_{4\pi} \frac{\Delta\widetilde{T} + \widetilde{Q}\tau/C}{1 + \Lambda\cos\theta i\xi_z + \Lambda\sin\theta\cos\phi i\xi_x + \Lambda\sin\theta\sin\phi i\xi_y} d\Omega \tag{3.145}$$

We convert the solid angel Ω into polar (θ) and azimuthal (ϕ) angle. For a very small solid angle $d\Omega$.

$$d\Omega = \sin\theta d\theta d\phi \tag{3.146}$$

Putting Equation 3.146 into Equation 3.145. We will get:

$$\Delta\widetilde{T} = \frac{1}{4\pi}\int_0^{2\pi}\int_0^{\pi} \frac{\Delta\widetilde{T} + \widetilde{Q}\tau/C}{1 + \Lambda\cos\theta i\xi_z + \Lambda\sin\theta\cos\phi i\xi_x + \Lambda\sin\theta\sin\phi i\xi_y} \sin\theta d\theta d\phi \tag{3.147}$$

To convert the integral of Equation 3.147 into an integratable form, we will use substitution method. Let us assume $\mu = \cos\theta$. The integral in Equation 3.147 will convert to:

$$\Delta\widetilde{T} = \frac{-1}{4\pi}\int_0^{2\pi}\int_1^{-1} \frac{\Delta\widetilde{T} + \widetilde{Q}\tau/C}{1 + \Lambda\mu i\xi_z + \Lambda\sqrt{1-\mu^2}\cos\phi i\xi_x + \Lambda\sqrt{1-\mu^2}\sin\phi i\xi_y} d\mu d\phi \tag{3.148}$$

$$\Delta\widetilde{T} = \frac{1}{4\pi}\int_0^{2\pi}\int_{-1}^{1} \frac{\Delta\widetilde{T} + \widetilde{Q}\tau/C}{1 + \Lambda\mu i\xi_z + \Lambda\sqrt{1-\mu^2}\cos\phi i\xi_x + \Lambda\sqrt{1-\mu^2}\sin\phi i\xi_y} d\mu d\phi \tag{3.149}$$

Solving the integral of Equation 3.149 using the identity given in Equation 3.150. We will get Equation 3.156

$$\boxed{\int \frac{1}{a + b\cos x + c\sin x} dx = \frac{2}{\sqrt{a^2 - b^2 - c^2}} \tan^{-1}\left(\frac{(a-b)\tan\frac{x}{2} + c}{\sqrt{a^2 - b^2 - c^2}}\right)} \tag{3.150}$$

Table 3.3: Coefficients of first integral

Coefficient	Value
a	$1 + \Lambda\mu i\xi_z$
b	$i\Lambda\xi_x\sqrt{1-\mu^2}$
c	$i\Lambda\xi_y\sqrt{1-\mu^2}$

$$\Delta\widetilde{T} = \frac{1}{4\pi}\int_{-1}^{1}\left[\frac{2(\Delta\widetilde{T} + \widetilde{Q}\tau/C)}{\sqrt{(1+\Lambda\mu i\xi_z)^2 - (i\Lambda\xi_x\sqrt{1-\mu^2})^2 - (i\Lambda\xi_y\sqrt{1-\mu^2})^2}}\right.$$
$$\left.\times \tan^{-1}\left(\frac{(1+\Lambda\mu i\xi_z - i\Lambda\xi_x\sqrt{1-\mu^2})\tan\frac{\phi}{2} + i\Lambda\xi_y\sqrt{1-\mu^2}}{\sqrt{(1+\Lambda\mu i\xi_z)^2 - (i\Lambda\xi_x\sqrt{1-\mu^2})^2 - (i\Lambda\xi_y\sqrt{1-\mu^2})^2}}\right)\right]_0^{2\pi} d\mu \tag{3.151}$$

$$= \frac{1}{4\pi}\int_{-1}^{1}\frac{2(\Delta\widetilde{T} + \widetilde{Q}\tau/C)}{\sqrt{1 + \Lambda^2(\xi_x^2 + \xi_y^2) + 2i\xi_z\Lambda\mu - \Lambda^2\xi^2\mu^2}}$$
$$\times\left[\tan^{-1}\left(\frac{(1+\Lambda\mu i\xi_z - i\Lambda\xi_x\sqrt{1-\mu^2})\tan\frac{\phi}{2} + i\Lambda\xi_y\sqrt{1-\mu^2}}{\sqrt{1 + \Lambda^2(\xi_x^2 + \xi_y^2) + 2i\xi_z\Lambda\mu - \Lambda^2\xi^2\mu^2}}\right)\right]_0^{2\pi} d\mu \tag{3.152}$$

$$= \frac{1}{4\pi}\int_{-1}^{1}\frac{2(\Delta\widetilde{T} + \widetilde{Q}\tau/C)}{\sqrt{1 + \Lambda^2(\xi_x^2 + \xi_y^2) + 2i\xi_z\Lambda\mu - \Lambda^2\xi^2\mu^2}}$$
$$\times\left[\tan^{-1}\left(\frac{(1+\Lambda\mu i\xi_z - i\Lambda\xi_x\sqrt{1-\mu^2})\tan\frac{\phi}{2} + i\Lambda\xi_y\sqrt{1-\mu^2}}{\sqrt{1 + \Lambda^2(\xi_x^2 + \xi_y^2) + 2i\xi_z\Lambda\mu - \Lambda^2\xi^2\mu^2}}\right)\right|_0^{\pi^-}$$
$$\left.+\tan^{-1}\left(\frac{(1+\Lambda\mu i\xi_z - i\Lambda\xi_x\sqrt{1-\mu^2})\tan\frac{\phi}{2} + i\Lambda\xi_y\sqrt{1-\mu^2}}{\sqrt{1 + \Lambda^2(\xi_x^2 + \xi_y^2) + 2i\xi_z\Lambda\mu - \Lambda^2\xi^2\mu^2}}\right)\right|_{\pi^+}^{2\pi} d\mu \tag{3.153}$$

$$
\begin{aligned}
&= \frac{1}{4\pi}\int_{-1}^{1} \frac{2(\Delta\widetilde{T}+\widetilde{Q}\tau/C)}{\sqrt{1+\Lambda^2(\xi_x^2+\xi_y^2)+2i\xi_z\Lambda\mu-\Lambda^2\xi^2\mu^2}} \\
&\times \Bigg[\tan^{-1}\left(\frac{(1+\Lambda\mu i\xi_z - i\Lambda\xi_x\sqrt{1-\mu^2})\tan(\frac{\pi^-}{2})+i\Lambda\xi_y\sqrt{1-\mu^2}}{\sqrt{1+\Lambda^2(\xi_x^2+\xi_y^2)+2i\xi_z\Lambda\mu-\Lambda^2\xi^2\mu^2}}\right) \\
&- \tan^{-1}\left(\frac{(1+\Lambda\mu i\xi_z - i\Lambda\xi_x\sqrt{1-\mu^2})\tan(0)+i\Lambda\xi_y\sqrt{1-\mu^2}}{\sqrt{1+\Lambda^2(\xi_x^2+\xi_y^2)+2i\xi_z\Lambda\mu-\Lambda^2\xi^2\mu^2}}\right) \\
&+ \tan^{-1}\left(\frac{(1+\Lambda\mu i\xi_z - i\Lambda\xi_x\sqrt{1-\mu^2})\tan(\pi)+i\Lambda\xi_y\sqrt{1-\mu^2}}{\sqrt{1+\Lambda^2(\xi_x^2+\xi_y^2)+2i\xi_z\Lambda\mu-\Lambda^2\xi^2\mu^2}}\right) \\
&- \tan^{-1}\left(\frac{(1+\Lambda\mu i\xi_z - i\Lambda\xi_x\sqrt{1-\mu^2})\tan(\frac{\pi^+}{2})+i\Lambda\xi_y\sqrt{1-\mu^2}}{\sqrt{1+\Lambda^2(\xi_x^2+\xi_y^2)+2i\xi_z\Lambda\mu-\Lambda^2\xi^2\mu^2}}\right)\Bigg] d\mu
\end{aligned} \tag{3.154}
$$

$$
\Delta\widetilde{T} = \frac{1}{4\pi}\int_{-1}^{1} \frac{2(\Delta\widetilde{T}+\widetilde{Q}\tau/C)}{\sqrt{1+\Lambda^2(\xi_x^2+\xi_y^2)+2i\xi_z\Lambda\mu-\Lambda^2\xi^2\mu^2}}\left[\frac{\pi}{2}+\frac{\pi}{2}\right] d\mu \tag{3.155}
$$

$$
\Delta\widetilde{T} = \frac{1}{2}\int_{-1}^{1} \frac{\Delta\widetilde{T}+\widetilde{Q}\tau/C}{\sqrt{1+\Lambda^2(\xi_x^2+\xi_y^2)+2i\xi_z\Lambda\mu-\Lambda^2\xi^2\mu^2}} d\mu, \tag{3.156}
$$

where $\xi = \sqrt{\xi_x^2+\xi_y^2+\xi_z^2}$. Let us solve the integral of Equation 3.156.

$$
I = \frac{1}{2}\frac{1}{\sqrt{1+\Lambda^2(\xi_x^2+\xi_y^2)+2i\xi_z\Lambda\mu-\Lambda^2\xi^2\mu^2}} d\mu, \tag{3.157}
$$

$$
\boxed{\int \frac{1}{\sqrt{a+bx+cx^2}}dx = \frac{-1}{\sqrt{-c}}\sin^{-1}\frac{2cx+b}{\sqrt{b^2-4ac}}} \tag{3.158}
$$

Solving integral (Equation 3.157) using the identity given in Equation 3.158. We will get:

Table 3.4: Coefficients of second integral

Coefficient	Value
a	$1+\Lambda^2(\xi_x+\xi_y)$
b	$2i\xi_z\Lambda\mu$
c	$-\Lambda^2\xi^2\mu^2$

$$
= \frac{-1}{2\sqrt{\Lambda^2\xi^2}}\sin^{-1}\frac{-2\Lambda^2\xi^2\mu+2i\xi_z}{\sqrt{(2i\xi_z\Lambda)^2-4((1+\Lambda^2(\xi_x^2+\xi_y^2))(-\Lambda^2\xi^2))}}\Bigg|_{\mu=-1}^{\mu=1} \tag{3.159}
$$

$$= \frac{-1}{2\sqrt{\Lambda^2\xi^2}} \sin^{-1} \frac{-2\Lambda^2\xi^2\mu + 2i\xi_z}{\sqrt{4\Lambda^2\xi^2 + 4\Lambda^4\xi^2(\xi_x^2+\xi_y^2) - 4\xi_z^2\Lambda^2}} \Bigg|_{\mu=-1}^{\mu=1} \tag{3.160}$$

$$= \frac{-1}{2\sqrt{\Lambda^2\xi^2}} \sin^{-1} \frac{-\Lambda\xi^2\mu + i\xi_z}{\sqrt{(\xi_x^2+\xi_y^2)(1+\Lambda^2\xi^2)}} \Bigg|_{\mu=-1}^{\mu=1} \tag{3.161}$$

$$= \frac{1}{2\sqrt{\Lambda^2\xi^2}} \sin^{-1} \frac{\Lambda\xi^2 + i\xi_z}{\sqrt{(\xi_x^2+\xi_y^2)(1+\Lambda^2\xi^2)}} - \frac{1}{2\sqrt{\Lambda^2\xi^2}} \sin^{-1} \frac{-\Lambda\xi^2 + i\xi_z}{\sqrt{(\xi_x^2+\xi_y^2)(1+\Lambda^2\xi^2)}} \tag{3.162}$$

$$= \frac{1}{2\sqrt{\Lambda^2\xi^2}} \left[\sin^{-1} \frac{\Lambda\xi^2 + i\xi_z}{\sqrt{(\xi_x^2+\xi_y^2)(1+\Lambda^2\xi^2)}} - \sin^{-1} \frac{-\Lambda\xi^2 + i\xi_z}{\sqrt{(\xi_x^2+\xi_y^2)(1+\Lambda^2\xi^2)}} \right] \tag{3.163}$$

Ler us simplify Equation 3.163 using identity given in Equation 3.164.

$$\sin^{-1} x - \sin^{-1} y = \sin^{-1} x\sqrt{1-y^2} - y\sqrt{1-x^2} \tag{3.164}$$

$$\begin{aligned} =& \frac{1}{2\Lambda\xi} \sin^{-1} \left[\frac{\Lambda\xi^2 + i\xi_z}{\sqrt{(\xi_x^2+\xi_y^2)(1+\Lambda^2\xi^2)}} \sqrt{1 - \frac{(-\Lambda\xi^2 + i\xi_z)^2}{(\xi_x^2+\xi_y^2)(1+\Lambda^2\xi^2)}} \right. \\ & \left. - \frac{-\Lambda\xi^2 + i\xi_z}{\sqrt{(\xi_x^2+\xi_y^2)(1+\Lambda^2\xi^2)}} \sqrt{1 - \frac{(\Lambda\xi^2 + i\xi_z)^2}{(\xi_x^2+\xi_y^2)(1+\Lambda^2\xi^2)}} \right] \end{aligned} \tag{3.165}$$

$$\begin{aligned} =& \frac{1}{2\Lambda\xi} \sin^{-1} \left[\frac{\Lambda\xi^2 + i\xi_z}{\sqrt{(\xi_x^2+\xi_y^2)(1+\Lambda^2\xi^2)}} \sqrt{\frac{(\xi_x^2+\xi_y^2)(1+\Lambda^2\xi^2) - (-\Lambda\xi^2 + i\xi_z)^2}{(\xi_x^2+\xi_y^2)(1+\Lambda^2\xi^2)}} \right. \\ & \left. - \frac{-\Lambda\xi^2 + i\xi_z}{\sqrt{(\xi_x^2+\xi_y^2)(1+\Lambda^2\xi^2)}} \sqrt{\frac{(\xi_x^2+\xi_y^2)(1+\Lambda^2\xi^2) - (\Lambda\xi^2 + i\xi_z)^2}{(\xi_x^2+\xi_y^2)(1+\Lambda^2\xi^2)}} \right] \end{aligned} \tag{3.166}$$

$$=\frac{1}{2\Lambda\xi}\sin^{-1}\left[\frac{\Lambda\xi^2+i\xi_z}{\sqrt{(\xi_x^2+\xi_y^2)(1+\Lambda^2\xi^2)}}\sqrt{\frac{\xi^2+\Lambda^2\xi^2(\xi_x^2+\xi_y^2)-\Lambda^2\xi^4+2i\xi_z\Lambda\xi^2}{(\xi_x^2+\xi_y^2)(1+\Lambda^2\xi^2)}}\right.$$
$$\left.-\frac{-\Lambda\xi^2+i\xi_z}{\sqrt{(\xi_x^2+\xi_y^2)(1+\Lambda^2\xi^2)}}\sqrt{\frac{\xi^2+\Lambda^2\xi^2(\xi_x^2+\xi_y^2)-\Lambda^2\xi^4-2i\xi_z\Lambda\xi^2}{(\xi_x^2+\xi_y^2)(1+\Lambda^2\xi^2)}}\right] \tag{3.167}$$

$$=\frac{1}{2\Lambda\xi}\sin^{-1}\left[\frac{\Lambda\xi^2+i\xi_z}{\sqrt{(\xi_x^2+\xi_y^2)(1+\Lambda^2\xi^2)}}\sqrt{\frac{\xi^2(1+\Lambda^2(\xi_x^2+\xi_y^2)-\Lambda^2\xi^2+2i\xi_z\Lambda)}{(\xi_x^2+\xi_y^2)(1+\Lambda^2\xi^2)}}\right.$$
$$\left.-\frac{-\Lambda\xi^2+i\xi_z}{\sqrt{(\xi_x^2+\xi_y^2)(1+\Lambda^2\xi^2)}}\sqrt{\frac{\xi^2(1+\Lambda^2\xi^2(\xi_x^2+\xi_y^2)-\Lambda^2\xi^2-2i\xi_z\Lambda)}{(\xi_x^2+\xi_y^2)(1+\Lambda^2\xi^2)}}\right] \tag{3.168}$$

$$=\frac{1}{2\Lambda\xi}\sin^{-1}\left[\frac{\Lambda\xi^2+i\xi_z}{\sqrt{(\xi_x^2+\xi_y^2)(1+\Lambda^2\xi^2)}}\sqrt{\frac{\xi^2(1+\Lambda\xi_z i)^2}{(\xi_x^2+\xi_y^2)(1+\Lambda^2\xi^2)}}\right.$$
$$\left.-\frac{-\Lambda\xi^2+i\xi_z}{\sqrt{(\xi_x^2+\xi_y^2)(1+\Lambda^2\xi^2)}}\sqrt{\frac{\xi^2(1-\Lambda\xi_z i)^2}{(\xi_x^2+\xi_y^2)(1+\Lambda^2\xi^2)}}\right] \tag{3.169}$$

$$=\frac{1}{2\Lambda\xi}\sin^{-1}\left[\frac{\xi(\Lambda\xi^2+i\xi_z)(1+i\Lambda\xi_z)-\xi(-\Lambda\xi^2+i\xi_z)(1-i\Lambda\xi_x)}{(\xi_x^2+\xi_y^2)(1+\Lambda^2\xi^2)}\right] \tag{3.170}$$

$$=\frac{1}{2\Lambda\xi}\sin^{-1}\left[\frac{\xi(i\xi_z+\Lambda\xi^2-\Lambda\xi_z^2+i\Lambda^2\xi_z\xi^2-i\xi_z+\Lambda\xi^2-\Lambda\xi_z^2-i\Lambda^2\xi_z\xi^2)}{(\xi_x^2+\xi_y^2)(1+\Lambda^2\xi^2)}\right] \tag{3.171}$$

$$=\frac{1}{2\Lambda\xi}\sin^{-1}\left[\frac{2\xi(\Lambda\xi^2-\Lambda\xi_z^2)}{(\xi_x^2+\xi_y^2)(1+\Lambda^2\xi^2)}\right] \tag{3.172}$$

$$=\frac{1}{2\Lambda\xi}\sin^{-1}\left[\frac{2\Lambda\xi(\xi_x^2+\xi_y^2)}{(\xi_x^2+\xi_y^2)(1+\Lambda^2\xi^2)}\right] \tag{3.173}$$

$$=\frac{1}{2\Lambda\xi}\sin^{-1}\left[\frac{2\Lambda\xi}{1+\Lambda^2\xi^2}\right] \tag{3.174}$$

$$= \frac{1}{\Lambda\xi}\frac{1}{2}\sin^{-1}\left[\frac{2\Lambda\xi}{\sqrt{1+\Lambda^2\xi^2}}\sqrt{1-\left(\frac{\Lambda\xi}{\sqrt{1+\Lambda^2\xi^2}}\right)^2}\right] \tag{3.175}$$

Ler us simplify Equation 3.175 using identity given in Equation 3.176.

$$2\sin^{-1}x = \sin^{-1}2x\sqrt{1-x^2} \tag{3.176}$$

$$= \frac{1}{\Lambda\xi}\sin^{-1}\left[\frac{\Lambda\xi}{\sqrt{1+\Lambda^2\xi^2}}\right] \tag{3.177}$$

$$I = \frac{1}{\Lambda\xi}\tan^{-1}\Lambda\xi \tag{3.178}$$

Putting value of integral (Equation 3.157) into Equation 3.158 and after rearranging, we will get the desired Green's function for steady state gray BTE.

$$\boxed{\Delta\widetilde{T} = \frac{\widetilde{Q}\tau}{C}\frac{\frac{1}{\Lambda\xi}\tan^{-1}(\Lambda\xi)}{1-\frac{1}{\Lambda\xi}\tan^{-1}(\Lambda\xi)}} \tag{3.179}$$

Analytical verification

Let us verify the obtained solution of gray BTE analytically by putting it back into the original Equation. For isotropical crystal the expanded steady state gray BTE is given in Equation 3.180.

$$v_g\cos\theta\frac{\partial e_\omega}{\partial z} + v_g\sin\theta\cos\phi\frac{\partial e_\omega}{\partial x} + v_g\sin\theta\sin\phi\frac{\partial e_\omega}{\partial y} - \frac{Q}{4\pi} = -\frac{e-e_o(T)}{\tau} \tag{3.180}$$

Computing the Fourier transform of both side of Equation 3.180. After re-arranging the terms, we will get:

$$v_g(\cos\theta i\xi_z + \sin\theta\cos\phi i\xi_x + \sin\theta\sin\phi i\xi_y)\widetilde{e} = -\frac{\widetilde{e}-\widetilde{e}_o(T)}{\tau} + \frac{\widetilde{Q}}{4\pi} \tag{3.181}$$

Integrating Equation 3.181 on both side over the solid angle Ω from 0 to 4π.

$$\int_{4\pi} v_g(\cos\theta i\xi_z + \sin\theta\cos\phi i\xi_x + \sin\theta\sin\phi i\xi_y)\widetilde{e}d\Omega = \int_{4\pi}\left[-\frac{\widetilde{e}-\widetilde{e}_o(T)}{\tau} + \frac{\widetilde{Q}}{4\pi}\right]d\Omega \tag{3.182}$$

Putting the value of energy density distribution function (e) given in Equation 3.143 and equilibrium energy density distribution function (e_o) given in Equation 3.128 into Equa-

tion 3.182. Solving for $L.H.S$, we will get:

$$\int_{4\pi} \frac{C}{4\pi} \frac{v_g(\cos\theta i\xi_z + \sin\theta\cos\phi i\xi_x + \sin\theta\sin\phi i\xi_y)}{1+\Lambda\cos\theta i\xi_z + \Lambda\sin\theta\cos\phi i\xi_x + \Lambda\sin\theta\sin\phi i\xi_y} \left(\Delta\widetilde{T} + \frac{\widetilde{Q}\tau}{C}\right) d\Omega \tag{3.183}$$

$$\int_{4\pi} \frac{C}{4\pi\tau} \frac{1+\Lambda\cos\theta i\xi_z + \Lambda\sin\theta\cos\phi i\xi_x + \Lambda\sin\theta\sin\phi i\xi_y - 1}{1+\Lambda\cos\theta i\xi_z + \Lambda\sin\theta\cos\phi i\xi_x + \Lambda\sin\theta\sin\phi i\xi_y} \left(\Delta\widetilde{T} + \frac{\widetilde{Q}\tau}{C}\right) d\Omega \tag{3.184}$$

$$\int_{4\pi} \frac{C}{4\pi\tau} \left(1 - \frac{1}{1+\Lambda\cos\theta i\xi_z + \Lambda\sin\theta\cos\phi i\xi_x + \Lambda\sin\theta\sin\phi i\xi_y}\right) \left(\Delta\widetilde{T} + \frac{\widetilde{Q}\tau}{C}\right) d\Omega \tag{3.185}$$

$$\frac{C}{4\pi\tau}\left(4\pi - \frac{4\pi}{\Lambda\xi}\tan^{-1}(\Lambda\xi)\right)\left(\Delta\widetilde{T} + \frac{\widetilde{Q}\tau}{C}\right) \tag{3.186}$$

Putting the value of $\Delta\widetilde{T}$ (Equation 3.179) into Equation 3.185. We have:

$$\frac{C}{\tau}\Big(1 - \frac{1}{\Lambda\xi}\tan^{-1}(\Lambda\xi)\Big)\Big(\frac{\widetilde{Q}\tau}{C}\frac{\frac{1}{\Lambda\xi}\tan^{-1}(\Lambda\xi)}{1-\frac{1}{\Lambda\xi}\tan^{-1}(\Lambda\xi)} + \widetilde{Q}\tau/C\Big) \tag{3.187}$$

$$\begin{aligned}\widetilde{Q}\frac{1}{\Lambda\xi}\tan^{-1}(\Lambda\xi) + \widetilde{Q} - \widetilde{Q}\frac{1}{\Lambda\xi}\tan^{-1}(\Lambda\xi)\\ = \widetilde{Q}\end{aligned} \tag{3.188}$$

Let us now compute the integral of $R.H.S$ of Equation 3.182.

$$\int_{4\pi}\left[-\frac{\widetilde{e}-\widetilde{e}_o(T)}{\tau} + \frac{\widetilde{Q}}{4\pi}\right]d\Omega \tag{3.189}$$

$$\int_{4\pi}\left[-\frac{\widetilde{e}-\widetilde{e}_o(T)}{\tau}\right]d\Omega + \int_{4\pi}\frac{\widetilde{Q}}{4\pi}d\Omega \tag{3.190}$$

Putting the value of equilibrium energy density distribution (Equation 3.128) into Equation 3.190. We will get:

$$-\int_{\Omega}\left[\frac{\widetilde{e}}{\tau} - \frac{1}{4\pi}\frac{C}{\tau}\Delta\widetilde{T}\right]d\Omega + \widetilde{Q} \tag{3.191}$$

First term of Equation 3.191 is same as Equation 3.132 which is zero. We will get:

$$= \widetilde{Q}$$

The $R.H.S$ and $L.H.S$ are equal so the gray BTE for steady state is verified.

3.2.2 Transient Analysis

Consider the gray BTE Equation 3.129, at transient the term $\partial e/\partial t$ will not be zero.

$$\frac{\partial e}{\partial t} + \vec{\boldsymbol{v}}_g.\nabla e - \frac{Q}{4\pi} = -\frac{e - e_o(T)}{\tau} \tag{3.192}$$

Solution

Putting Equation 3.126 and 3.128 into gray BTE Equation 3.192 and computing the Fourier transform of both side. We will get:

$$(i\eta + v_g\cos\theta i\xi_z + v_g\sin\theta\cos\phi i\xi_x + v_g\sin\theta\sin\phi i\xi_y)\widetilde{e} = -\frac{\widetilde{e}}{\tau} + \frac{C}{4\pi\tau}\Delta\widetilde{T} + \frac{\widetilde{Q}}{4\pi}, \tag{3.193}$$

where $\sim$ represents the Fourier transform, i is equal to $\sqrt{-1}$, and η is the temporal frequency. Rearranging Equation 3.193, we will have:

$$\widetilde{e} = \frac{C}{4\pi}\frac{\Delta\widetilde{T} + \widetilde{Q}\tau/C}{1 + i\eta\tau + \Lambda\cos\theta i\xi_z + \Lambda\sin\theta\cos\phi i\xi_x + \Lambda\sin\theta\sin\phi i\xi_y}. \tag{3.194}$$

Putting Equation 3.194 into Equation 3.132 and after rearranging we will get:

$$\Delta\widetilde{T} = \frac{1}{4\pi}\int_{4\pi}\frac{\Delta\widetilde{T} + \widetilde{Q}\tau/C}{1 + i\eta\tau + \Lambda\cos\theta i\xi_z + \Lambda\sin\theta\cos\phi i\xi_x + \Lambda\sin\theta\sin\phi i\xi_y}d\Omega \tag{3.195}$$

We convert the solid angel Ω into polar(θ) and azimuthal(ϕ) angle. For a very small solid angle $d\Omega$.

$$d\Omega = \sin\theta d\theta d\phi \tag{3.196}$$

Putting Equation 3.146 into Equation 3.197. We will get:

$$\widetilde{T} = \frac{1}{4\pi}\int_0^{2\pi}\int_0^{\pi}\frac{\Delta\widetilde{T} + \widetilde{Q}\tau/C}{1 + i\eta\tau + \Lambda\cos\theta i\xi_z + \Lambda\sin\theta\cos\phi i\xi_x + \Lambda\sin\theta\sin\phi i\xi_y}\sin\theta d\theta d\phi \tag{3.197}$$

To convert the integral of Equation 3.197 into an integrable form, we will use substitution method. Let us assume $\mu = \cos\theta$. The integral in Equation 3.197 will convert to:

$$\Delta\widetilde{T} = \frac{-1}{4\pi}\int_0^{2\pi}\int_1^{-1}\frac{\Delta\widetilde{T} + \widetilde{Q}\tau/C}{1 + i\eta\tau + \Lambda\mu i\xi_z + \Lambda\sqrt{1-\mu^2}\cos\phi i\xi_x + \Lambda\sqrt{1-\mu^2}\sin\phi i\xi_y}d\mu d\phi \tag{3.198}$$

$$\Delta\widetilde{T} = \frac{1}{4\pi}\int_0^{2\pi}\int_{-1}^{1}\frac{\Delta\widetilde{T} + \widetilde{Q}\tau/C}{1 + i\eta\tau + \Lambda\mu i\xi_z + \Lambda\sqrt{1-\mu^2}\cos\phi i\xi_x + \Lambda\sqrt{1-\mu^2}\sin\phi i\xi_y}d\mu d\phi \tag{3.199}$$

Solving the integral of Equation 3.199 using the identity given in the Equation 3.150. We will get the Equation 3.200

$$\Delta\widetilde{T} = \frac{1}{2}\int_{-1}^{1} \frac{\Delta\widetilde{T} + \widetilde{Q}\tau/C}{\sqrt{1-\eta^2\tau^2 + 2i\eta\tau + 2i\Lambda\xi_z\mu - 2\eta\xi_z\tau\Lambda\mu + \Lambda^2(\xi_x^2+\xi_y^2) - \Lambda^2\xi^2\mu^2}} d\mu, \quad (3.200)$$

where $\xi = \sqrt{\xi_x^2+\xi_y^2+\xi_z^2}$. Solving the integral of Equation 3.200 using the identity given in Equation 3.158. We will get the desired Green's function for transient gray BTE.

$$\boxed{\Delta\widetilde{T} = \frac{\widetilde{Q}\tau}{C}\frac{\frac{1}{\Lambda\xi}\tan^{-1}\left(\frac{\Lambda\xi}{1+i\eta\tau}\right)}{1-\frac{1}{\Lambda\xi}\tan^{-1}\left(\frac{\Lambda\xi}{1+i\eta\tau}\right)}} \quad (3.201)$$

Analytical verification

Let us verify the obtained solution of gray BTE analytically by putting it back into the original Equation. For isotropical crystal the expanded steady state gray BTE is given in Equation 3.202.

$$\frac{\partial e}{\partial t} + v_g\cos\theta\frac{\partial e_\omega}{\partial z} + v_g\sin\theta\cos\phi\frac{\partial e_\omega}{\partial x} + v_g\sin\theta\sin\phi\frac{\partial e_\omega}{\partial y} - \frac{Q}{4\pi} = -\frac{e-e_o(T)}{\tau} \quad (3.202)$$

Computing the Fourier transform of both side of Equation 3.202. After re-arranging the terms, we will get:

$$\left(i\eta + v_g(\cos\theta i\xi_z + \sin\theta\cos\phi i\xi_x + \sin\theta\sin\phi i\xi_y)\right)\widetilde{e} = -\frac{\widetilde{e}-\widetilde{e}_o(T)}{\tau} + \frac{\widetilde{Q}}{4\pi} \quad (3.203)$$

Integrating the Equation 3.203 on both side over the solid angle Ω form 0 to 4π.

$$\int_{4\pi}\left(i\eta + v_g(\cos\theta i\xi_z + \sin\theta\cos\phi i\xi_x + \sin\theta\sin\phi i\xi_y)\right)\widetilde{e}d\Omega = \int_{4\pi}\left[-\frac{\widetilde{e}-\widetilde{e}_o(T)}{\tau} + \frac{\widetilde{Q}}{4\pi}\right]d\Omega \quad (3.204)$$

Putting the value of energy density distribution (e) given in Equation 3.194 and equilibrium energy density distribution function(e_o) given in Equation 3.128 into Equation 3.204. Solving for $L.H.S$, we will get:

$$\int_{4\pi}\frac{C}{4\pi}\frac{i\eta + v_g(\cos\theta i\xi_z + \sin\theta\cos\phi i\xi_x + \sin\theta\sin\phi i\xi_y)}{1+i\eta\tau + \Lambda\cos\theta i\xi_z + \Lambda\sin\theta\cos\phi i\xi_x + \Lambda\sin\theta\sin\phi i\xi_y}\left(\Delta\widetilde{T} + \frac{\widetilde{Q}\tau}{C}\right)d\Omega \quad (3.205)$$

$$\int_{4\pi}\frac{C}{4\pi\tau}\frac{1+i\eta\tau + \Lambda\cos\theta i\xi_z + \Lambda\sin\theta\cos\phi i\xi_x + \Lambda\sin\theta\sin\phi i\xi_y - 1}{1+i\eta\tau + \Lambda\cos\theta i\xi_z + \Lambda\sin\theta\cos\phi i\xi_x + \Lambda\sin\theta\sin\phi i\xi_y}\left(\Delta\widetilde{T} + \frac{\widetilde{Q}\tau}{C}\right)d\Omega \quad (3.206)$$

$$\int_{4\pi} \frac{C}{4\pi\tau}\left(1-\frac{1}{1+i\eta\tau+\Lambda\cos\theta i\xi_z+\Lambda\sin\theta\cos\phi i\xi_x+\Lambda\sin\theta\sin\phi i\xi_y}\right)\left(\Delta\widetilde{T}+\frac{\widetilde{Q}\tau}{C}\right)d\Omega \tag{3.207}$$

$$\frac{C}{\tau}\left(4\pi-\frac{4\pi}{\Lambda\xi}\tan^{-1}\left(\frac{\Lambda\xi}{1+i\eta\tau}\right)\right)\left(\Delta\widetilde{T}+\frac{\widetilde{Q}\tau}{C}\right) \tag{3.208}$$

$$\frac{C}{\tau}\Big(1-\frac{1}{\Lambda\xi}\tan^{-1}\left(\frac{\Lambda\xi}{1+i\eta\tau}\right)\Big)\Big(\frac{\widetilde{Q}\tau}{C}\frac{\frac{1}{\Lambda\xi}\tan^{-1}\left(\frac{\Lambda\xi}{1+i\eta\tau}\right)}{1-\frac{1}{\Lambda\xi}\tan^{-1}\left(\frac{\Lambda\xi}{1+i\eta\tau}\right)}+\widetilde{Q}\tau/C\Big) \tag{3.209}$$

$$\begin{aligned}\widetilde{Q}\frac{1}{\Lambda\xi}\tan^{-1}\left(\frac{\Lambda\xi}{1+i\eta\tau}\right)+\widetilde{Q}-\widetilde{Q}\frac{1}{\Lambda\xi}\tan^{-1}\left(\frac{\Lambda\xi}{1+i\eta\tau}\right)\\ =\widetilde{Q}\end{aligned} \tag{3.210}$$

Let now compute the integral of $R.H.S$ of Equation 3.204.

$$\int_{4\pi}\left[-\frac{\widetilde{e}-\widetilde{e}_o(T)}{\tau}+\frac{\widetilde{Q}}{4\pi}\right]d\Omega \tag{3.211}$$

$$\int_{4\pi}\left[-\frac{\widetilde{e}-\widetilde{e}_o(T)}{\tau}\right]d\Omega+\int_{4\pi}\frac{\widetilde{Q}}{4\pi}d\Omega \tag{3.212}$$

Putting the value of equilibrium energy density distribution function (Equation 3.128) into Equation 3.190. We will get:

$$-\int_{\Omega}\left[\frac{\widetilde{e}}{\tau}-\frac{1}{4\pi}\frac{C}{\tau}\Delta\widetilde{T}\right]d\Omega+\widetilde{Q} \tag{3.213}$$

First term of the Equation 3.213 is same as Equation 3.132 which is zero. We will get:

$$=\widetilde{Q}$$

The $R.H.S$ and $L.H.S$ are equal so the gray BTE for transient is verified.

3.3 Combined Solution

We compute the base temperature profile of the chip by convolving the Fourier Green's function with the power profile of the chip, and then we use this thermal profile to compute the temperature of 1000×1000 nm^2 blocks using the BTE based Green's function (see Figure 3.4). This gives us the temperature profile of regions of interest: standard cells, and small functional units.

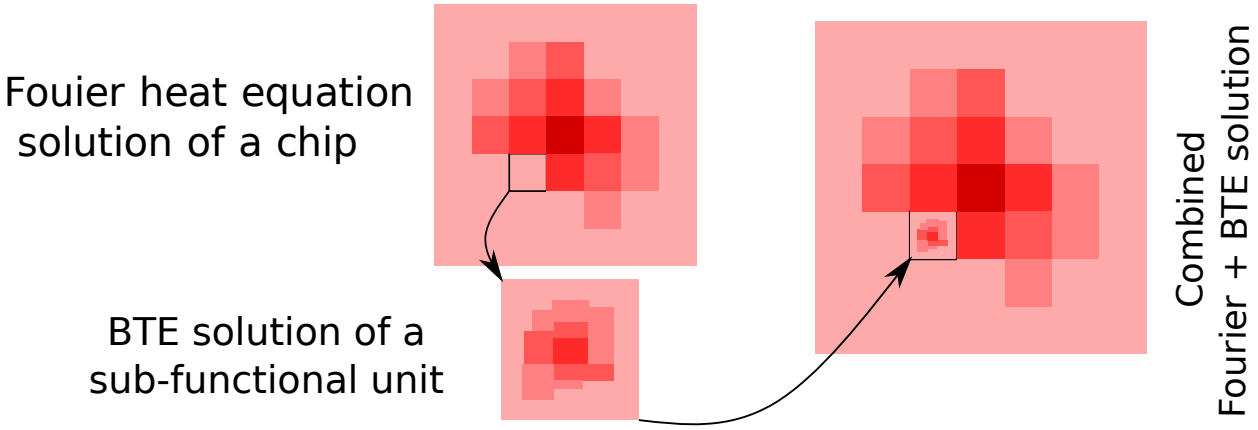

Figure 3.4: Fourier-Boltzmann framework

Chapter 4

Evaluation

4.1 Setup

We run the simulations on an Intel i7 3^{rd}generation processor based desktop with 8GB RAM running Ubuntu 18.04. For validating our Fourier analysis results, we used a commercial CFD simulator COMSOL (Version 5.3b) [31], and we compare our BTE solution against ThermalScope (available as *ISAC2*). The Fourier solution was done in R (version 3.5.1), and the BTE solution was done on Matlab 17b.

Error Metric: We have reported the root mean square (RMS) value of the error for all the test cases. Where percentage errors are reported, these are relative to the maximum temperature rise (similar to [11]). In ThermalScope the authors report the average error (average error is always less than the RMS error).

4.2 Fourier Analysis

We run the Fourier steady-state simulation for a chip with a heat spreader on top of it. The chip and heat spreader dimensions are $10\ mm \times 10\ mm \times 0.15\ mm$ and $10\ mm \times 10\ mm \times 3.52\ mm$ [12, 4] respectively. The conductivity of silicon and the heat spreader is $150\ W/mK$ and $256\ W/mK$ respectively (it is the effective conductivity of the heat spreader and the TIM).

4.2.1 Steady State

Green's function based full chip temperature calculation can be broken down into two parts [2, 10, 12]:

1. Green's function computation (offline)
2. Full chip thermal profile computation (online)

Green's function: We have calculated the Green's function assuming the source to be a circle of finite radius applied at the center of the chip (to exploit the symmetry of the thermal distribution).

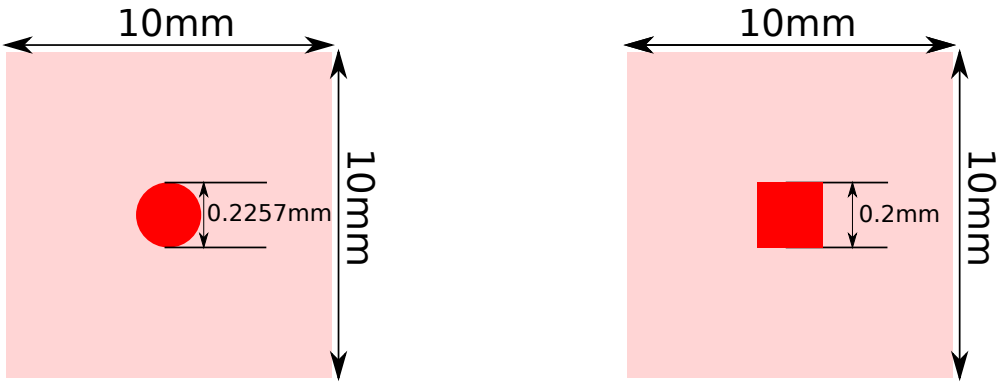

(a) (b)

Figure 4.1: (a) Circular source (b) Square source

However, the floorplan elements in a real chip are rectangular; they can only be discretized into small square grid points. Thus we need a way of mapping these square grid points to circular sources (for which we calculate the Green's function). For this, we take a circular source of equal area as the square source. We sample the continuous Green's function at the centers of the grid points determined by discretizing the chip into a grid. We have found that a grid size of 0.2 mm provides sufficient accuracy for a chip of area 100 mm^2 or more (Figure 4.1). Similar discretizations were found to be sufficient in [4]. The RMS error obtained by this approximation is $0.023°C$, which is small enough compared to the maximum temperature rise of $17°C$ (maximum error of 1.7%). Figure 4.2 shows the comparison of the calculated Green's function (using the circular source) against the Green's function obtained in COMSOL (using a square source of equal area).

Our implementation takes 0.082 s to compute the Green's function for a 10×10 mm^2 chip. We also calculated the Green's function using COMSOL for the same configuration, and observed a simulation time of 305 s. Other Green's function based simulators such as LightSim [10, 12] and PowerBlurring [4] depend on FEM based simulators for the calculation of the Green's function. If the geometry of the chip or the boundary conditions change, the Green's function will have to be recomputed. In our work, since we analytically obtain the Green's function, our approach gives designers the *flexibility to experiment with the package*, as there is no dependence on any external tool.

Full Chip Thermal Profile: We computed the thermal profile for four test cases (Figure 4.3 and 4.4). In the first two test cases we discretized a 10×10 mm^2 chip into a 50×50 grid. Test cases 3 and 4 have been implemented to evaluate our algorithm on two real floorplans.

Test Case 1: In this case, we have applied power sources at the center and all corners of the chip. This represents one of the worst case power profiles possible, since the corners and edges contribute to a large part of the error in Green's function based approaches [4].

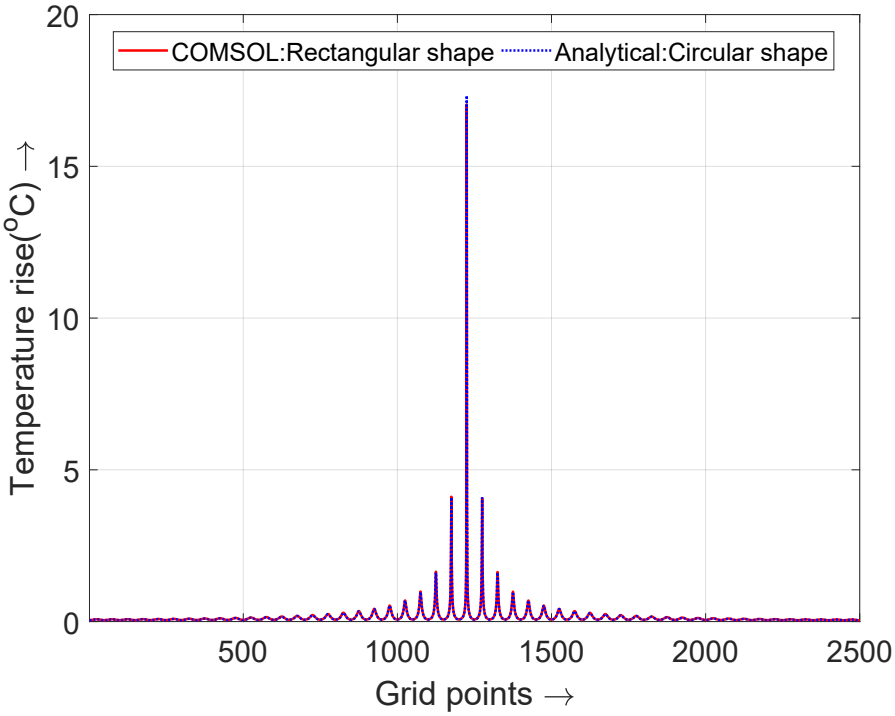

Figure 4.2: Comparison of *NanoTherm* and COMSOL (Fourier, steady state Green's function)

We obtained an RMS error of $0.046°C$ (maximum error 1.57%) compared to COMSOL (Figure 4.3b). This verifies our corners and edge correction approach.

Test Case 2: This test case is similar to Test case 1, except that the power densities are much higher here ($2500\ W/cm^2$). We have used a very high power density figure to evaluate our algorithm for extreme cases anticipated in next generation processors [32]. An RMS error of $0.169°C$ (maximum error 2.88%) was observed in comparison to COMSOL.

Test Case 3: We have further evaluated our algorithm using the floorplan of a processor containing a single core of Alpha21264 and an L2 cache. The dimensions of the processor are $16\ mm \times 16\ mm \times 0.15\ mm$. The core has 15 functional units. The power density of each functional unit is shown in Figure 4.4a (obtained from HotSpot). The calculated thermal profile of the chip is shown in Figure 4.4b. An RMS error of $0.047°C$ (maximum error 3.2%) was observed against the COMSOL model. This error is greater than that of test cases 1 and 2, since all the major sources have been placed along an edge of the processor.

Test Case 4: We have also implemented a dual-core processor in 45 nm technology based on the Intel Gainestown architecture [33]. Each core is divided into six sub-units, and all cores share an L3 cache. The power density of each block is shown in Figure 4.4c. The size of the processor is $11.2\ mm \times 11.2\ mm \times 0.15\ mm$. The calculated thermal profile is shown in Figure 4.4d. An RMS error of $0.099°C$ (maximum error 1.9%) was observed against the

COMSOL model.

Runtime: The total runtime of the algorithm was 83.5 ms for all the test cases (including the Green's function computation time). We need only 1.5 ms in the online stage to compute the full chip temperature profile, by taking the FFT of the Green's function and the power profile and computing the inverse transform of the product. To compute the same steady state thermal profile, COMSOL requires 305 s. Thus *NanoTherm* provides a speedup of $3652X$ over COMSOL.

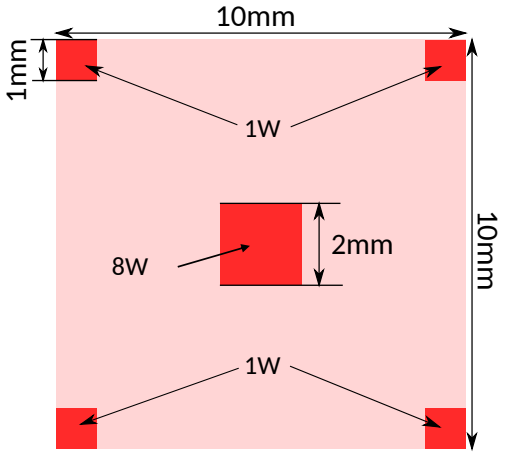

(a) Power distribution

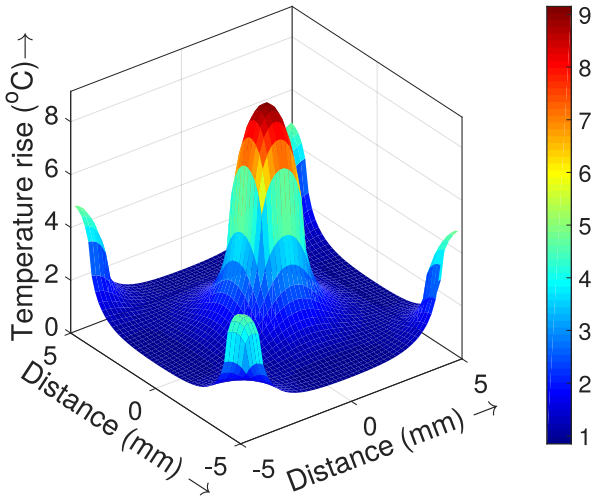

(b) Thermal profile

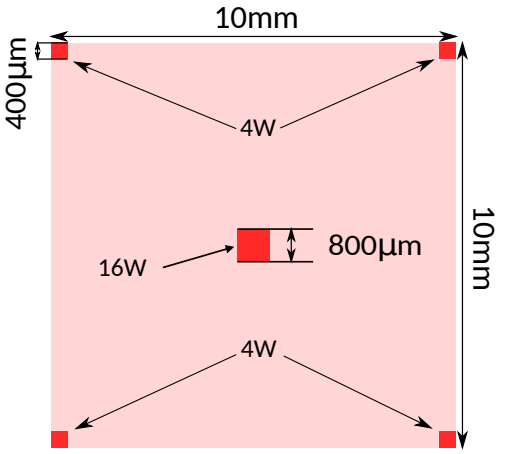

(c) Power distribution

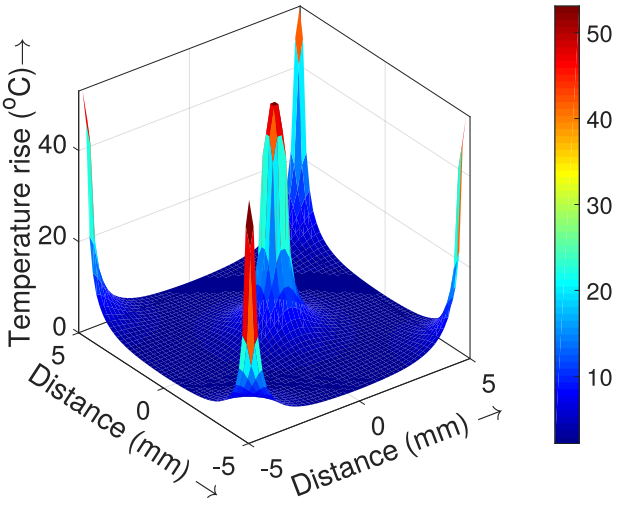

(d) Thermal profile

Figure 4.3: Power and thermal profiles for test cases 1 and 2

Transient:

For transient analysis, we use the same setup. The density of silicon and the heat spreader are 2330 kg/m^3 and 8960 kg/m^3 respectively, and the specific heat values are 700 $J/kg.K$

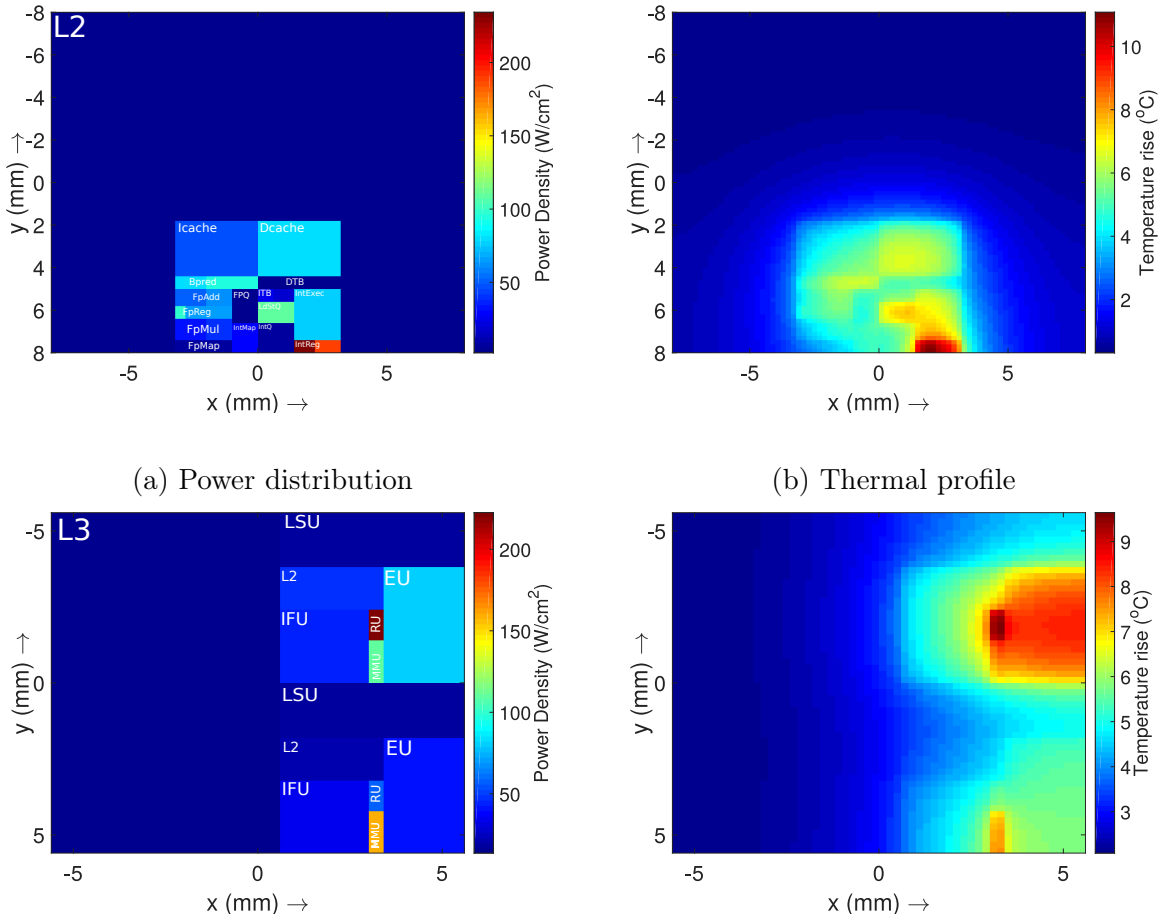

(a) Power distribution

(b) Thermal profile

(c) Power distribution

(d) Thermal profile

Figure 4.4: Evaluation for Alpha21264 and Gainestown architectures

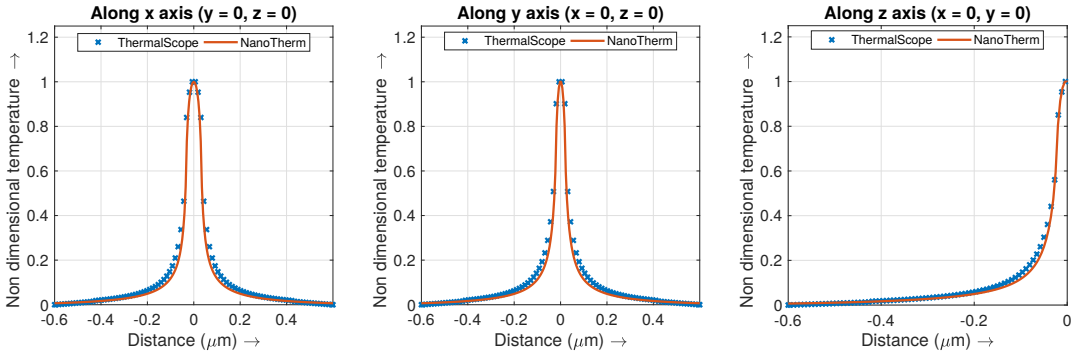

Figure 4.5: Comparison of *NanoTherm* and ThermalScope (BTE, steady state)

and 390 $J/kg.K$ respectively.

Step response: We start with applying a 1 W step source at the center of the chip. We calculated the step response of the chip for 100 radial points and 40-time steps. The runtime of the algorithm was 4.15 s (Note: 25% of the time is going in the slow inverse Laplace

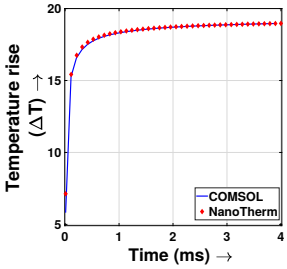

Figure 4.6: Comparison of *NanoTherm* and COMSOL (Fourier, transient)

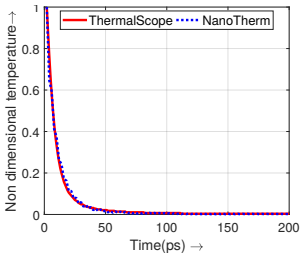

Figure 4.7: Comparison of *NanoTherm* and ThermalScope (BTE, transient)

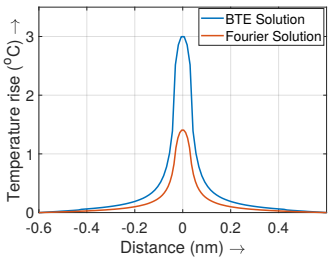

Figure 4.8: Comparison of Fourier and BTE (steady state)

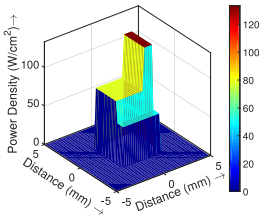

Figure 4.9: Power distribution

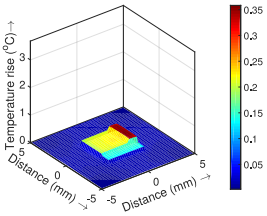

Figure 4.10: ΔT at t = 0.01 ms

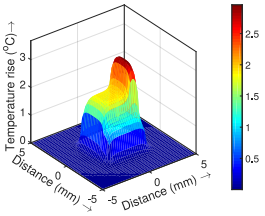

Figure 4.11: ΔT at t = 2 ms

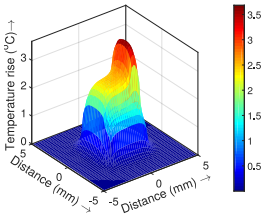

Figure 4.12: ΔT at t = 4 ms

transform routine of R). Also, *NanoTherm* has been implemented in R whereas HotSpot and 3DICE have been implemented in C++. R is several times slower than C++ [34], and hence, the implementation of *NanoTherm* in C++ or any other similar language would be faster. In comparison, for calculating the same step response, COMSOL took 3005 s (*NanoTherm* is faster by roughly $724X$). Figure 4.6 compares the accuracy of our transient simulation against COMSOL, where the error is limited to 1%.

Full Chip Thermal Profile: We compute the transient thermal profile of a $10 \times 10\ mm^2$ chip for the power profile given in Figure 4.9. The calculated thermal profiles at time instants t = 0.01 ms, $2ms$, and $4ms$ are shown in Figure 4.10, 4.11, and 4.12 respectively. An RMS error of $0.057°C$ was observed for t = 4 ms. A total simulation time of 4.2 s was observed. To compute the same transient thermal profile COMSOL took 3005 s (speedup of $715X$).

4.2.2 BTE Analysis:

We compare the BTE steady state solution against the Fourier steady state solution for a 60 $nm \times 45\ nm \times 20nm$ channel FET. Solving the Fourier equation only results in a maximum error of $1.59°C$ or 53% (Figure 4.8), similar to [16].

Steady State

We run the simulation for steady state BTE with a 60 $nm \times 45\ nm \times 20nm$ channel FET [13, 15]. A simulation time of 3.3 s was observed for $400 \times 400 \times 200$ grid points. In comparison the steady state simulation in ThermalScope takes 36.76 min (speedup of $641X$). An RMS error of $0.06°C$ was observed against the ThermalScope. Figure 4.5 compares the results of *NanoTherm* and ThermalScope.

Transient

We used the same steady state configuration for the transient simulation as well. A simulation time of 39.5 s was observed for 200 time steps. We run the same simulation with ThermalScope with the same meshing (as we had for steady state) and the simulation time observed was 48.1 min. An RMS error of $0.087°C$ was observed. Figure 4.7 compares the result of *NanoTherm* and ThermalScope.

4.2.3 Simulation Speed

Table 4.1 summarizes the time needed to compute the temperature profile for all cases (chip level and nanometer level, steady state and transient) by popular commercial and open source tools. The time taken by COMSOL to obtain the steady state thermal profile was 305 s. Therefore our algorithm is $3652X$ faster than COMSOL. We are 7X faster than ThermalScope in calculating the transient Fourier solution. For BTE solution, we are $668X$ faster than ThermalScope while calculating the steady state profile and 73X faster in computing the transient thermal profile.

Table 4.1: Speed of popular simulators

Simulator	Fourier heat eq		BTE	
	Steady	Transient	Steady	Transient
Hotspot[1]	1 s	36 s	-	-
3DICE	1.36 s	1.77 s	-	-
COMSOL	305 s	3005 s	-	-
ThermalScope	11.1 s	32.55 s	2206 s	2888 s
NanoTherm	0.083s	4.2s	3.3s	39.5s

[1] For an acceptable accuracy in Hotspot and 3DICE, a grid size of $\sim 128 \times 128$ is used.
[2] HotSpot, 3D-ICE and COMSOL do not solve the BTE.

Chapter 5

Conclusion

State of the art thermal estimation techniques either do not take the nanoscale quantum effects into account, or solve for these effects using the slower finite element method. In this paper, we propose a fast and analytical thermal estimation technique that incorporates nanoscale quantum effects as well. We solve the Fourier equation analytically using a Green's function based approach and speed up the process by exploiting the symmetry of the heat distribution. Further, we solve the Boltzmann transport equation analytically and combine it with the Fourier solution to propose an analytical full chip thermal estimation framework. Our results show that we are 7-668X faster than the state of the art tool, ThermalScope, with an error limited to 3%.

Bibliography

[1] Y. Zhan and S. S. Sapatnekar, "A high efficiency full-chip thermal simulation algorithm," in *ICCAD-2005. IEEE/ACM International Conference on Computer-Aided Design, 2005.*, pp. 635–638, IEEE, 2005.

[2] Y. Zhan and S. S. Sapatnekar, "Fast computation of the temperature distribution in vlsi chips using the discrete cosine transform and table look-up," in *Proceedings of the 2005 Asia and South Pacific Design Automation Conference*, pp. 87–92, ACM, 2005.

[3] P. Michaud, Y. Sazeides, A. Seznec, T. Constantinou, and D. Fetis, *An analytical model of temperature in microprocessors.* PhD thesis, INRIA, 2005.

[4] A. Ziabari, J.-H. Park, E. K. Ardestani, J. Renau, S.-M. Kang, and A. Shakouri, "Power blurring: Fast static and transient thermal analysis method for packaged integrated circuits and power devices," *IEEE Transactions on Very Large Scale Integration (VLSI) Systems*, vol. 22, no. 11, 2014.

[5] E. Gondro, O. Kowarik, G. Knoblinger, and P. Klein, "When do we need non-quasistatic cmos rf-models?," in *Proceedings of the IEEE 2001 Custom Integrated Circuits Conference (Cat. No. 01CH37169)*, pp. 377–380, IEEE, 2001.

[6] W.-L. Hung, G. M. Link, Y. Xie, N. Vijaykrishnan, and M. J. Irwin, "Interconnect and thermal-aware floorplanning for 3d microprocessors," in *International Symposium on Quality Electronic Design*, pp. 6–pp, IEEE, 2006.

[7] J.-M. Lin, T.-T. Chen, Y.-F. Chang, W.-Y. Chang, Y.-T. Shyu, Y.-J. Chang, and J.-M. Lu, "A fast thermal-aware fixed-outline floorplanning methodology based on analytical models," in *2018 IEEE/ACM International Conference on Computer-Aided Design (ICCAD)*, pp. 1–8, IEEE, 2018.

[8] K. Skadron, M. R. Stan, W. Huang, S. Velusamy, K. Sankaranarayanan, and D. Tarjan, "Temperature-aware microarchitecture," in *30th Annual International Symposium on Computer Architecture, 2003. Proceedings.*, pp. 2–13, IEEE, 2003.

[9] J.-H. Park, A. Shakouri, and S.-M. Kang, "Fast evaluation method for transient hot spots in vlsi ics in packages," in *9th International Symposium on Quality Electronic Design (isqed 2008)*, pp. 600–603, IEEE, 2008.

[10] S. R. Sarangi, G. Ananthanarayanan, and M. Balakrishnan, "Lightsim: A leakage aware ultrafast temperature simulator," in *2014 19th Asia and South Pacific Design Automation Conference (ASP-DAC)*, pp. 855–860, IEEE, 2014.

[11] A. Sridhar, A. Vincenzi, M. Ruggiero, T. Brunschwiler, and D. Atienza, "3d-ice: Fast compact transient thermal modeling for 3d ics with inter-tier liquid cooling," in *2010 IEEE/ACM International Conference on Computer-Aided Design (ICCAD)*, pp. 463–470, IEEE, 2010.

[12] H. Sultan and S. R. Sarangi, "A fast leakage aware thermal simulator for 3d chips," in *Proceedings of the Conference on Design, Automation & Test in Europe*, pp. 1737–1742, European Design and Automation Association, 2017.

[13] Z. Hassan, N. Allec, F. Yang, L. Shang, R. P. Dick, and X. Zeng, "Full-spectrum spatial–temporal dynamic thermal analysis for nanometer-scale integrated circuits," *IEEE Transactions on Very Large Scale Integration (VLSI) Systems*, vol. 19, no. 12, pp. 2276–2289, 2011.

[14] C. Hua and A. J. Minnich, "Analytical green's function of the multidimensional frequency-dependent phonon boltzmann equation," *Physical Review B*, vol. 90, no. 21, p. 214306, 2014.

[15] S. V. Narumanchi, J. Y. Murthy, and C. H. Amon, "Boltzmann transport equation-based thermal modeling approaches for hotspots in microelectronics," *Heat and mass transfer*, vol. 42, no. 6, pp. 478–491, 2006.

[16] N. Allec, Z. Hassan, L. Shang, R. P. Dick, and R. Yang, "Thermalscope: Multi-scale thermal analysis for nanometer-scale integrated circuits," in *Proceedings of the 2008 IEEE/ACM International Conference on Computer-Aided Design*, pp. 603–610, IEEE Press, 2008.

[17] S. Mazumder and A. Majumdar, "Monte carlo study of phonon transport in solid thin films including dispersion and polarization," *Journal of Heat Transfer*, vol. 123, no. 4, pp. 749–759, 2001.

[18] A. Nabovati, D. P. Sellan, and C. H. Amon, "On the lattice boltzmann method for phonon transport," *Journal of Computational Physics*, vol. 230, no. 15, pp. 5864–5876, 2011.

[19] C. Hua and A. J. Minnich, "Heat dissipation in the quasiballistic regime studied using the boltzmann equation in the spatial frequency domain," *Physical Review B*, vol. 97, no. 1, p. 014307, 2018.

[20] S. Zahiri, C. Shao, Y. Shen, and H. Bao, "Collocation mesh-free method to solve the gray phonon boltzmann transport equation," *Numerical Heat Transfer, Part B: Fundamentals*, vol. 70, no. 5, pp. 459–471, 2016.

[21] B. Wang and P. Mazumder, "Accelerated chip-level thermal analysis using multilayer green's function," *Computer-Aided Design of Integrated Circuits and Systems, IEEE Transactions on*, vol. 26, no. 2, pp. 325–344, 2007.

[22] A. K. Coşkun, J. L. Ayala, D. Atienza, and T. S. Rosing, "Thermal modeling and management of liquid-cooled 3d stacked architectures," in *IFIP/IEEE International Conference on Very Large Scale Integration-System on a Chip*, pp. 34–55, Springer, 2009.

[23] J.-H. Park, S. Shin, J. Christofferson, A. Shakouri, and S.-M. Kang, "Experimental validation of the power blurring method," in *2010 26th Annual IEEE Semiconductor Thermal Measurement and Management Symposium (SEMI-THERM)*, pp. 240–244, IEEE, 2010.

[24] P. Mittal, "Integral transforms for engineers and physicists," 2007.

[25] Weisstein and E. W, "Hankel Transform, From MathWorld–a Wolfram Resource." `http://mathworld.wolfram.com/HankelTransform.html`. Accessed: 2019-02-30.

[26] H. Flanders, "Differentiation under the integral sign," *The American Mathematical Monthly*, vol. 80, no. 6, pp. 615–627, 1973.

[27] Weisstein and E. W, "Bromwich Integral, From MathWorld–a Wolfram Resource." `http://mathworld.wolfram.com/BromwichIntegral.html`. Accessed: 2019-02-13.

[28] F. N. Donmezer, D. Singh, W. James, A. Christensen, S. Graham, and J. Y. Murthy, "Lattice boltzmann and discrete ordinates methods for phonon transport modeling: A comparative study," in *ASME 2011 International Mechanical Engineering Congress and Exposition*, pp. 333–343, American Society of Mechanical Engineers, 2011.

[29] R. A. Escobar, S. S. Ghai, M. S. Jhon, and C. H. Amon, "Multi-length and time scale thermal transport using the lattice boltzmann method with application to electronics cooling," *International Journal of Heat and Mass Transfer*, vol. 49, no. 1-2, pp. 97–107, 2006.

[30] A. Majumdar, "Microscale heat conduction in dielectric thin films," *Journal of Heat Transfer*, vol. 115, no. 1, pp. 7–16, 1993.

[31] COMSOL, "Comsol 5.3b cfd tool." `https://www.comsol.com/release/5.3a`, 2018. Accessed: 2018-09-30.

[32] F. Kaplan, M. Said, S. Reda, and A. K. Coskun, "Locool: Fighting hot spots locally for improving system energy efficiency," *IEEE Transactions on Computer-Aided Design of Integrated Circuits and Systems*, 2019.

[33] P. Gepner, D. L. Fraser, and M. F. Kowalik, "Second generation quad-core intel xeon processors bring 45 nm technology and a new level of performance to hpc applications," in *International Conference on Computational Science*, pp. 417–426, Springer, 2008.

[34] S. B. Aruoba and J. Fernández-Villaverde, "A comparison of programming languages in economics," tech. rep., National Bureau of Economic Research, 2014.

LIST OF PAPERS BASED ON THESIS

1. NanoTherm: An Analytical Fourier-Boltzmann Framework for Full Chip Thermal Simulations, Shashank Varshney, Hameedah Sultan, Palkesh Jain, Smruti R. Sarangi. International Conference on Computer Aided Design (ICCAD), Westminister, USA